

KFK 2889  
Dezember 1979

# The Role of Gases in Radiation Damage Patterns

D. Kaletta  
Institut für Material- und Festkörperforschung

Kernforschungszentrum Karlsruhe



KERNFORSCHUNGSZENTRUM KARLSRUHE

Institut für Material- und Festkörperforschung

KfK 2889

The Role of Gases in Radiation Damage Patterns

D. Kaletta

Kernforschungszentrum Karlsruhe GmbH, Karlsruhe

Als Manuskript vervielfältigt  
Für diesen Bericht behalten wir uns alle Rechte vor

Kernforschungszentrum Karlsruhe GmbH  
ISSN 0303-4003

## Summary

### The Role of Light Gases in Radiation Damage Patterns

The paper reviews the radiation damage phenomena in metals after light element irradiation, in particular helium. The irradiation-induced defects, the microstructural damages associated, and the changes in mechanical properties induced are discussed in terms of the homologous temperature and the CTR-parameter combining the amount of atoms injected and the amount of damage created. Particular attention is paid to the atomistic approach to describing small-size effects. Large-size effects, currently created in a phenomenological manner, are discussed in the last section and the phenomena of gas re-emission, gas bubbles in the bulk and surface bubbles are considered in some detail.

## Zusammenfassung

### Die Bedeutung leichter Gase für Strahlenschäden

Der Artikel berichtet über Strahlenschäden in Metallen nach Implantation leichter Ionen, im besonderen Helium. Die strahlungs-induzierten Defekte, die damit verbundenen mikrostrukturellen Schäden und die Änderungen der mechanischen Eigenschaften werden in Termen der homologen Temperatur und des Fusionsreaktor-Parameters diskutiert, der das Verhältnis der implantierten Atome zu dem hervorgerufenen Schaden angibt. Eine spezielle Betrachtung erfährt die atomistische Näherung zur Beschreibung von Effekten im submikroskopischen Bereich. Mikroskopische Effekte, die gegenwärtig nur phänomenologisch behandelt werden, sind Bestandteil des letzten Abschnittes, wobei die Phänomene der Gas-Reemission, der Volumen-Gasblasen und der Oberflächenblasen im einzelnen diskutiert werden.

## 1. Introduction

It cannot be the aim of a short review to cover the areas on which a light particle beam can impinge. The energy range of beams available today from several eV to several billions of eV makes it necessary to cut the questions of interest and to select topics on the subject of radiation damage in materials for a fusion reactor and to the experience of the speaker.

Thus, the objective of my talk is to highlight the effects caused by light particles in metals after irradiation-induced displacements of lattice-atoms. In 1943, Wigner predicted the displacement of lattice-atoms by neutrons. The critical energy for displacement, the Wigner energy, is about 25 eV. In metals and we shall use the term "irradiation", here, when primary collision events ensure displacements of lattice-atoms and the incorporation of the implanted or knocked-on particles, i.e. the target is thick enough compared to the mean penetration depth.

The maximum energy transferred,

$$T_{\max} = \frac{4A_1A_2}{(A_1+A_2)^2} \quad (1)$$

$A_i$  = atomic mass of  
the particles

must therefore be higher than the displacement energy. Thus, in the case of neutrons the kinetic energy is above 400 eV and in the case of electrons above some 100 KeV. Due to sputtering and other surface-related effects energies below some KeV are not considered in the case of light ions. Above some KeV effects were excluded, when the objective of implantation is to use the beam as a diagnostic tool, as is done in backscattering experiments, for example. In the high-energy range, when the ion energy exceeds the coulomb barrier

$$B[\text{MeV}] = \frac{Z_1Z_2}{A_2^{1/2}} \quad (2)$$

$Z_i$  = atomic number  
of the particles

we disregard beam effects, if they were established for particle generation. Thus, the remaining window - and it is still large enough -

is the "classical" implantation range from some KeV to some 1000KeV and the effects considered are radiation damage phenomena in terms of displacements and incorporations. Classically, light ions are ions with mass numbers below 4. i.e. the paper will mainly treat the hydrogen and helium bombardment. As far as necessary for comparison and illustration, ions with atomic numbers below 10 will also be considered.

The second part of the paper summarizes the principal features of radiation damage in metals concerning high dose effects (dose >  $10^{20}/m^2$ ). The atomistic approach to describing small-size effects is presented in the third part, whilst large-size effects currently treated in a phenomenological manner are discussed in the final part.

## 2. Radiation damage phenomena - a brief course

The basis of the interest in light element implantation in metals is the tremendous development of nuclear technology primarily leading to the actual or potential construction of power stations based on fission or fusion neutrons. The nucleation and growth for radiation-induced damage structures in reactors first observed by Cawthorne and Fulton /1/ has promoted fundamental studies of the damage caused by the agglomeration of Frenkel-defects. Due to long-term irradiation in neutron facilities irradiations simulating the damage in short-term experiments have been enforced. As is shown in Fig. 1, even light particles, such as electrons or hydrogen ions, are much more powerful in creating displacement damage than neutron. Thus, the irradiation time can be reduced by several orders of magnitude in non-neutron experiments.

The problems of simulation, however, are well known /2,3/ and can be classified as follows.

- (1) An increasing displacement rate shifts the nucleation onset to higher temperatures /4/. For example, the difference in temperature is about 150 K when comparing heavy ion and neutron irradiations at 800 K irradiation temperature in the neutron-experiment. At equivalent fluences the test material therefore is in a different material state.
- (2) The differences in the primary recoil spectra generated by these particles shown in Fig. 2 according to Ref. /5/ influence the nucleation behaviour due to different levels of the free, irradiation-induced vacancy concentration /6/. In the case of electrons single Frenkel-pairs, i.e. a self-interstitial and a vacancy, are generated, while in the case of heavy-ions the vacancies generated are bound in cascades partially.
- (3) Simple simulation experiments using beams of one species cannot take into account the influence of hydrogen and helium, or of transmutation products in general, on damage which is observed experimentally /7 - 9/ and is under theoretical discussion /10/. In the case of helium a drastic increase in the nucleation rate by several orders of magnitude can be claimed and the stability of vacancy-rich cavities containing helium is enhanced. Apart from this scaling behaviour, the incorporation of hydrogen and, especially, helium extends the radiation damage patterns and new phenomena are observed exclusively related to these species.

Light particle irradiations which are connected with the voidage problem and which can be characterized as scaling-experiments are not considered. Phenomena which are attributed to displacements and gas incorporation and which can be studied by light gas implantations are treated.

In nuclear environments the gases are generated by nuclear reactions of (n,p)- and (n, $\alpha$ )-type, in ion implantation facilities the gases were implanted directly. In the case of a Tokamak-type fusion reactor implantations and transmutations occur simultaneously, since the (d,t)-plasma reaction produces free alpha-particles as well as 14-MeV neutrons. Assuming currently available particle fluxes, i.e.  $10^{18}$  particles per  $m^2$  and second, the rate  $K_g$  at which the gas is generated or implanted in metals is shown in the first table. The unit is gas-atom per lattice-atom and second, abbreviated (gpa/s). Analogous to the gas rate, the displacement rate  $K_v$  can be defined by counting the number of displaced atoms per lattice-atom and second in units of (dpa/s). In the case of neutron irradiations, the displacement rate given in Tab. 1 consists of damage events caused by primary knocked-on atoms, i.e. lattice-atoms, mainly. The self-damage induced by the transmutation products contributes a few percent as seen in Fig. 3. Here, according to Parkin and Goland /6/, the damage energy is split into the different generation processes and only at high neutron energies the inelastic scatter-parts contribute significantly. In ion implantation facilities, however, the damage is pure self-damage generated along the penetration path of the ion. Fig. 4 shows the helium deposition profile assumed to be Gaussian and the displacement curve calculated by a modified EDEP-1 code /11, 12/ in terms of the elastic energy loss for helium in vanadium at different energies.

The origin of incorporation, however, is important for the kinetic behaviour of the ions after having come to rest. Disregarding the initial phase of irradiation, in the case of neutron bombardment all gaseous transmutations are generated in a lake of vacancies enlarged by the relatively small self-damage, i.e. under conditions, where the steady-state level of vacancies differs from thermal equilibrium. The quasi-homogeneous distribution of irradiation-induced vacancies is a consequence of the quasi-isotropic scattering-law of neutrons and their infinite range for nonabsorbing targets. In the case of ion implantations, usually normal to one target surface, both the deposited ions and the damage show the depth-dependence as seen in Fig. 4. It is convenient and also supported by certain experimental techniques of damage analysis /12/ to define five depth layers of different concentration gradients:

- (I) a near-surface layer with a small helium and vacancy concentration,
- (II) a damage layer with high vacancy concentration and increasing helium concentration,
- (III) an implantation layer with high helium concentration and decreasing vacancy concentration,
- (IV) an end-of-range layer with decreasing helium and vacancy concentration, and
- (V) the undamaged matrix layer.

In order to discuss radiation phenomena on the basis of synergistic effects as occurring under neutron irradiation and multiple beam irradiation /13, 14/, a CTR-parameter (controlled thermonuclear reactor) was introduced recently /9/ combining the amount of a transmutation product with the damage created. In the case of helium, for example, the parameter has the dimension of (appm He/dpa). The next Fig. 5 displays the depth-dependence of this parameter for helium implanted in vanadium. Although the CTR-parameter represents a quantity useful for a first orientation in radiation damage phenomena, it cannot explain or predict the detailed behaviour of implanted structures. For quantitative discussion of the damage observed after irradiation the actual vacancy concentration must be known which, in principle, can be calculated by using diffusion model techniques.

In a first stage, Bullough /15/ used a coupled set of partial differential equations of parabolic order. The general form treats the damage rate (enhanced by the defect rate of thermally created defects) as a source term and the diffusion-controlled mutual recombination of interstitials and vacancies as well as the defect lost at lattice-defects of the first order, i.e. dislocations, as sink terms.

The steady-state solution predicts, for example, at what temperatures a vacancy supersaturation is expected and what its amount is, as illustrated in Fig. 6 /16/. Refined models as introduced by Sizmann et al. /17/ and Foreman /18/, taking into account the near-surface as a sink term, even give a good indication of the amount of damage remaining after irradiation, as long as self-ion bombardment is considered, for example, silver ions in silver. In the presence of light ions, these simple equation sets fail, but nevertheless, they estimate the maximum damage available after irradiation. Fig. 7 gives an example /12/. According to this calculation, helium-vacancy agglomerations are formed up to depths of  $1 \mu\text{m}$  only, but, experimentally, the largest helium bubbles are observed beyond this depth /12/.

Although understanding of the underlying physical behaviour of radiation damage phenomena seems to be sufficient for explanation, a general theory still fails, due to the complexity of the bombarded material. This holds even for pure metals, since the dislocation structure, the grain-boundary structure and the chemical sensitivity to impurities such as carbon, nitrogen and oxygen play an important and often a dominant role for the resulting damage structure /19,20/ and in the case of alloys, the number of metallurgical effects can be increased in an arbitrary manner by effects of the second order, i.e. precipitations, by alloy instabilities etc. It is no joke, but rather a cause for alarm that the intrinsic state of materials of technological interest such as stainless steel, resembles an exploded drugstore.

In order to reduce or even avoid these difficulties, physicists started to irradiate metals of the highest purity at temperatures below that of liquid nitrogen. The irradiation-induced defects were frozen and any thermal interaction among the defects and between the defects and the microstructure of the material was inhibited. Athermal effects, such as the displacement energy or the spontaneous recombination volume of induced Frenkel-pairs could be established /21/ and after isochronic heat treatments below 300 K the diffusion behaviour of single interstitials and vacancies could be determined from, mostly, resistivity measurements /22/. In excellent experiments questions of state of configuration of the defects were investigated and, in part, verified. These low-temperature experiments

are well documented /23/, but with increasing temperature of heat treatment, the relatively simple structures disappear and the business of thermally activated migration and agglomeration above 300 K sets in.

Disregarding thermal effects for a moment, energy transfers much greater than the displacement energy lead to branching collision paths and therefore to collision cascades. These spikes or depleted zones first postulated by Brinkmann /24/, refined by Seeger /25/, and now under intense study /26, 27/. occur preferentially as faulted loops on the close-packed lattice-planes, irrespectively of the stacking-fault energy on these lattice-planes. Typical diameters of these cascades lie between some nm and some 10 nm depending on mass, atomic number and packing density of the lattice-atoms. Cascade diameters and distances of cascade centres from the irradiation surface can be calculated, e.g., by the theory of Winterbon et al. /28/. Fig. 8 shows a displacement spike according to Seeger /25/.

Due to the vacancy-rich core of these cascades, it is assumed that they are important for the nucleation of larger cavities /29, 30/. From theoretical calculations there is some indication that also in the case of light ion impacts cascades can be generated, but their sizes are very small, thus implying difficult experimental investigations. Presently the open literature contains studies for atom numbers above 10, only. We shall leave this area, therefore, although the formation of cascades is highly important in large-size defect growth.

Let us now come to the main part of this paper, namely, the behaviour of implanted gases in metals under thermal conditions allowing defect migration. The next figure, Fig. 9, highlights the different defect structures observed as a function of temperature ( $T > 300$  K) and the CTR-parameter. On a rough scale, three temperature regions and three CTR-parameter regions can be distinguished.

$$T < 0.35 T_m$$

In the low-temperature region between 0.15 and 0.35  $T_m$  ( $T_m$  = melting point temperature in Kelvin), where helium as well as the vacancies are nearly immobile, the microstructure consists of a high density of vacancy and/or interstitial defect clusters or dislocation loops, typically a few nm in diameter /35/, Fig. 10. At high CTR-parameters, attainable only by ion irradiations, the growth of helium-vacancy complexes begins above a critical density leading to a surface deformation called blistering /31/, as is shown in Fig. 11, /12/. The formation and growth of these irradiation-induced lattice defects cause matrix-hardening depending on the size and number of these defects which, in turn, are temperature- and dose-dependent. For the case of cubic body-centered materials, additively, the transition temperature from brittle to ductile fracture can be increased, as has been confirmed experimentally for molybdenum /32/.

$$0.35 < T/T_m < 0.57$$

Above 0.35  $T_m$ , the vacancies become mobile and the thermally activated absorption and reemission of vacancies and interstitials controls the growth behaviour of irradiation-induced defects.

At low CTR-parameters, where the ratio  $g/v$  of the number of gas atoms ( $g$ ) to vacancies ( $v$ ) is small in a cavity compared to 0.25, the vacancies precipitate to form voids and the interstitials form a dislocation structure. At low doses and temperatures in this range, the dislocation structure generally consists of faulted loops which increase in size with increasing dose and temperature and may unfault forming a dislocation network /33, 34/. Fig. 12 shows well aligned loops after 673 K helium implantation in nickel /35/ and Fig. 13 the temperature-dependence of voids formed after bombardment with 20 MeV C ions /36/.

With increasing CTR-parameter the local concentration of helium increases and it is assumed that the cavities can be characterized by bubbles obeying a gas law /37, 38/, for example, a van-de-Waals law. From a theoretical point of view, the distinction between a bubble,

i.e. a gas-filled cavity, and a void, i.e. a nearly empty cavity, can easily be made by specifying the  $g/v$ -value. In practice, however, a separation is not possible, although due to stability criteria the high-temperature annealing of both defects should be different. Thus, the term "bubble" is reserved for cavities observed after rare gas implantations, especially helium, whereas the term "void" is used for pores after non rare gas implantations. In Fig. 14 a bubble population is seen corresponding to different sample depths, i.e. to different CTR-parameters /39/.

At very high CTR-parameters, again, blistering is observed /40/, as seen in Fig. 15, but now accompanied by large bubbles.

The ductility losses found at the lower end of this temperature range recover with increasing temperature in the absence of helium. If helium, however, is present in noticeable concentration, high-temperature embrittlement due to helium clusters formed and/or bubbles along grain-boundaries is observed and the failure mode changes from intragranular to intergranular fracture /37, 39/, Fig. 16.

$$T > 0.57 T_m$$

The point defects are not stable in this high temperature region and diffusion is controlled by the thermal vacancies. The helium bubbles, however, grow to large cavities until they are able to cut the target surface, Fig. 17. This perforation accompanied by strong gas reemission takes place above a threshold dose (6,40.1). Below this critical dose, only gas reemission is observed. The mechanical behaviour of the material can be described in terms of high-temperature embrittlement.

Most of the defects described in Fig. 9 are well documented for pure vanadium. They can be observed in nearly all metals and their occurrence depends on temperature and the CTR-parameter as scaled in Fig. 9. In detail, the defect-shape, its size, its concentration, and its interaction with existing lattice defects sensitively depend on the actual material and irradiation parameters and cannot presently be predicted quantitatively. Even small additions of interstitial impurities, such as C, O or N in

B.C.C. metals can alter their radiation defect patterns. The next figure, Fig. 18, illustrates such differences in simple binary alloying for V - 20 % Ti /39/: the bulk bubbles, mostly cubic in shape for pure V, become elongated and are formed preferentially at precipitates and grain-boundaries and the surface bubbles observed in pure V are replaced by large exfoliations along grain-boundaries.

The analogous figure of radiation damage in the case of hydrogen bombardment is simpler due to the high solubility of hydrogen in most of the metals. Four types of damages have been observed: voidage (at high proton energies above 0.1 MeV), gas reemission, surface deformation and hydrogen embrittlement. Apart from the void formation, all phenomena are low-temperature effects, becoming significant below  $0.3 T_m$ .

This paper will not treat the complications introduced by the presence of precipitations. The first experiments performed to study their formation and dissolution under irradiation systematically are either neutron experiments or heavy ion implantations /40.2, 40.3/. Nevertheless, if present, they play an important role for the nucleation and growth of irradiation defects.

### 3. The atomistic approach in describing small-size defects

In the recent years, a number of theoretical studies on the migration of helium and hydrogen in the common F.C.C. and B.C.C. metals have been written and received excellent reviews (for example, /41/). Those studies were largely based on atomistic calculations simulating the crystal processes by using an atomic model for the lattice and computing the equations of motion of each atom as the lattice is subjected to an external perturbation. The results of these calculations are picked-up, here, from the viewpoint of applicability to radiation damage processes described in Fig. 9, by mentioning the methods of calculation just superficially.

In an early treatment Johnson /42/ modelled a spherical crystallite of 530 atoms surrounded by an elastic continuum. Using an interaction potential for iron he calculated vacancy formation and migration energies together with eight stable interstitial configurations. His calculations illustrated the need for carefully determined interaction potentials. The first method of approach is to consider the gas-metal interactions to be comprised of two-body potentials, where the helium particle with its closed and tightly bound electron shell is simpler to consider from an interaction standpoint than the open-shell hydrogen atom. A functional form for the interaction might be chosen with parameters which are fitted to experimental data such as cohesive energy, interatomic separation, bulk-modulus, elastic constants, phonon dispersion curves, etc.. Thus was done first by Rimmer and Cottrell /43/ who averaged a helium-helium potential and the Huntington copper-copper potential fitted to crystal data in such a way that the resulting potential is the minimum obtained upon variation of the copper and helium radii. The limitation of this approach is that at all interatomic distances except near equilibrium, where the potential is matched, it is extrapolated. Applied to gas-metal or defect-metal interactions, the calculations are powerful in developing broad behavioural patterns as done by Johnson /44/ rather than in specifying precise activation energies, since data concerning the interactions of the impurity or defect with the lattice do not exist. A more fundamental calculation must, therefore, be performed.

Ab initio calculations were developed by Wilson and Bisson /45/ and were used in atomistic calculations of the behaviour of helium. They mainly compared their results for interstitial helium migration in copper with calculations using a number of existing semi-empirical and other Cu-Cu potentials. The activation energies ranged from 0.45 to 0.71 eV demonstrating, however, a relative insensitivity to potentials employed in the case of copper, in the case of the B.C.C. metals V, Fe, Mo, Ta, and W it was generally found that interstitial activation energies were in the  $< 0.25$  eV range, approximately half that obtained in Cu. Conversely, the interstitial formation energies in B.C.C. metals are about a factor of two higher than in copper, but such formation energies lead to such low solubilities that the difference may not be experimentally verifiable.

Practically, it means that even parts of 1 appm helium implanted represent a supersaturation of helium far from thermal equilibrium conditions. The heavier gases (He-Xe) possess sufficient interstitial formation energies to generate Frenkel defects /43, 46/. Thus, krypton and xenon are able to move easily from an interstitial position (for the heaviest gases a split interstitial configuration /46/) by forming a Frenkel defect, whereas helium should reside interstitially or diffuse out of the lattice depending on its migration energy, unless it is trapped at pre-existing defects. In well-annealed pure vanadium such a long-range migration was observed at relatively low doses and temperature /12/. Neither the irradiation-induced vacancies nor thermally created vacancies existed at such concentrations as to act as a significant trap for this high-flux irradiation. The helium was stopped by the grain-boundaries forming bubbles there far beyond the mean penetration depth. No bubbles were found around the damage and the helium peak as usually observed at higher doses and temperatures.

The fast interstitial migration of helium turns into a slow substitutional motion, if a vacancy is present to act as a trap. Wilson and coworkers discussed the properties of complex defect configurations called clusters, (g,v), in Tungsten /47/ and Copper /48/. For Cu they calculated the binding energies for clusters up to ten helium atoms in up to four vacancies. In the case of gas-clustering in adjacent interstitial positions the binding energies are found to be low, less than 0.2 eV which is the maximum value for a (3,0)-cluster. The sixth atom is not bound at all. Thus, if interstitial clustering occurs at all, it is not a predominant effect and it is unimportant at room temperatures and above. Adding just one vacancy drastically changes the situation. Fig. 19 shows the state of configuration of these clusters. The two helium atoms in the (2,1)-cluster share the vacancy and lie along a (100)-direction, equidistant at  $0.46 r_0$  ( $r_0$  = half lattice constant) and the second helium is bound to the (1,1)-cluster by 0.79 eV. The most stable poly-atomic gas cluster is the (6,1)-cluster, where again the helium atoms occupy (100)-positions each at  $0.73 r_0$  from the vacancy. The sixth gas atom is bound by 0.86 eV to the existing cluster of five. In general the binding of the  $n$ -th helium atom in a vacancy cluster tends to decrease as a function of  $n$ , whereas the binding energy of an  $m$ -th vacancy tends to increase with

helium content. Clusters with  $m = n$  represent a most stable configuration with a vacancy binding of 1.27 eV and a helium binding of 1.84 eV as is seen in Table 2 according to Wilson et al. /48/. This means, that such clusters are stable up to  $0.4 T_m$ .

The nucleation time and the concentration of the clusters are very sensitive to the helium migration energy /12/. At low activation energies mixed clusters of about equal numbers of gas atoms and vacancies were nucleated preferentially, whilst the nucleation of helium rich clusters in general dominates at high migration energies. Several processes for helium motion have to be taken into account. The fastest motion is the interstitial motion mentioned above which takes place at an energy of 0.29 eV in tungsten, for example /49/. Where the gas diffuses as a substitutional impurity its motion is controlled by a very high activation energy of 5.1 eV in W, for example /49/. Helium occupying a divacancy is highly mobile. In the case of copper Wilson and Bisson /50/ found, that the migration energy of an empty divacancy of 0.47 eV just increases to 0.74 eV when containing a helium atom which is close to the interstitial migration energy of 0.55 eV for helium in copper. Due to the easy dissociation of divacancies, it is assumed that the migration of an occupied divacancy consists of a sequence of steps: in the first one a (1,1)-cluster picks-up a vacancy, migrates and dissociates leaving a (1,1)-cluster, again collects a vacancy etc.. A so-called popout mechanism for substitutional helium motion was proposed by Wilson and Johnson /51/, where the gas jumps from a substitutional to an interstitial position. In this position the gas is free to diffuse until encountering another vacancy. The activation energy for the substitutional de-trapping is consistently high, somewhat larger in B.C.C. metals than in F.C.C. metals. On a first-order, this energy is the difference of the formation energies of He in interstitial and substitutional position and it is lower than the activation energy for self-diffusion as seen in Table 3 which shows some migration energies for helium clusters in Tungsten according to Refs. /49, 51/. Recently de Hosson et al. /52/ examined the edge dislocation as a helium trapping site. The migration energy of 0.4 eV in molybdenum and Tungsten chosen as model materials does not differ appreciably from the bulk-value, thus providing the possibility of pipe-diffusion along the perfect edge dislocation perpendicular to the (112) plane with a

Burgers vector of  $1/2 [111]$  in that plane. The binding of helium on an edge dislocation is nearly half of what it is in a vacancy.

Resolution of a helium cluster by displacement due to self-interstitials has been reported by Wilson and Bisson /53/. Single helium-vacancy as well as poly-atomic helium-vacancy clusters up to (5,1) are not able to prevent a Frenkel-apir recombination, and an effective self-interstitial capture volume of 250 atomic volumes was found /54/. Clusters containing more than one vacancy are found to combine rapidly with self-interstitials above 300 K. Thus, helium clustering is an important catalyst for the formation of a void or a bubble due to the reduction of strains surrounding the cluster by absorbing vacancies, but, on the other hand, helium resolution could dramatically control void or bubble nucleation rates.

Applying the cluster results to ion irradiation experiments at temperatures where the defects are mobile, Baskes and Wilson /55/ used their set of 42 coupled first-order rate equations and allowed self-interstitials, helium interstitials, vacancies and di-vacancies to diffuse. They compared their calculation with 50 KeV helium implantations in Copper /56/ determining the amount of helium retained after annealing. The interesting feature is the breakup of the (6,1)-cluster with temperature in such a way, that the concentration of cluster containing more helium is centered around and beyond the mean penetration depth, whereas helium-poorer clusters are concentrated towards the surface. The existence of clusters with high helium content and enormous strain-fields has been proposed by Kaletta /3, 40/ as an assumption for the stress-induced growth of bubbles found in the region beyond the peak. The growth is thought to be caused by an ejection of an intervening lattice atom for strain reduction.

#### 4. The phenomenological approach to describing large-size defects

It was mentioned that the CTR-parameter as defined in sect. 2 just outlines the damage structures qualitatively. The damage quantities, however, are determined by the magnitudes of the damage induced and the gas atoms incorporated at fixed conditions. The dependence on dose is not linear for all defects formed by a gas-metal interaction, i.e., bubble formation, blistering and gas reemission, for example /57/. Generally, these defects are high-dose effects and their occurrence is observed above a critical dose. In this section some results obtained in pure materials are presented in order to achieve substantial understanding of the mechanism controlling the behavioural patterns of these defects. Metallurgical effects, though important, are omitted.

##### 4.1 Gas reemission in metals after helium and hydrogen implantation

The term "reemission" collects a number of processes by which trapped ions can be released. The pre-existing lattice damage of a metal plays an important role in discussing the mechanism involved in reemission spectra. The lattice damage increases the trapping efficiency as was shown by Kornelson /58/ who studied the desorption rates of helium implanted at a sub-threshold energy of 250 eV in an annealed tungsten lattice and in a tungsten lattice predamaged by 5 KeV krypton ions. By deconvoluting the desorption spectra, Kornelson associated the population of individual sites varying in different powers in the incident ion dose to different helium-vacancy clusters discussed in the last section.

Helium reemission after high-energy helium implantation has been studied by Bauer and Thomas in a wide variety of metals such as niobium /59/, molybdenum /60/, vanadium /60/, stainless steel /60/ and aluminium /61/. Erents and McCracken also measured the reemission rates from molybdenum /62/. However, in none of these investigations were the results analysed in the same detail as in the case of tungsten. From these high-energy implantation experiments a basic pattern of behaviour has emerged. Three distinct, temperature dependent modes of helium release are exhibited. Fig. 20 illustrates the results found by Wilson and Thomas /63/ in aluminium bombarded with 20 KeV helium ions.

At a very low temperature ( $0.1 T_m$ ) the reemission data show a period of high gas retention until a critical dose of  $3 \times 10^{17}/\text{cm}^2$  was achieved, followed by a steady rise in the reemission rate. 100 % reemission indicates release at the implantation rate. The intermediate temperature regime ( $0.2 - 0.4 T_m$ ) was characterized by sudden bursts of helium. At high temperature ( $> 0.5 T_m$ ) a third type of gas reemission is found. The helium release again becomes a steady and smooth curve after an initial period of gas retention, but the  $0.5 T_m$  implant has a shorter interval of gas retention and a more rapid approach to a steady-state release rate compared to the low-temperature release. The period of gas retention shows a dependence on material and temperature, but it is rather insensitive to the microstructures studied. At all modes of helium release a surface deformation was observed to be characteristic for each stage. It will be discussed in Sec. 4.3.

The trapping of hydrogen behaves differently from that of helium, since it has a high diffusion coefficient and a high solubility in most metals. A model for the out-diffusion of hydrogen during implantation has been discussed by Erents and McCracken /64/ valid for chemically nonreactive metals. It is based on an equilibrium gradually set up between the incident ions and the outgoing gas. The surface is considered to be a sink for diffusing atoms causing a steeper concentration gradient towards the surface than to the bulk. Qualitatively the experimental curves were similar to the predicted form, but the values of diffusion coefficient required to fit the curves were about two orders of magnitude below those measured in conventional thermal diffusion experiments, where hydrogen is interstitially migrating. The difference was attributed to a trapping effect of hydrogen /65/ rather similar to that for helium. The principal difference between hydrogen and helium is that the binding energy of hydrogen is considerably lower than helium and that hydrogen is observed to be in interstitial sites /66/.

The temperature dependence of gas release shows the steady and smooth curve behaviour up to high temperatures after a retention period. The length of the period shortens, when the temperature is increased /67/. At low temperatures a surface deformation is observed indicating that the local solubility is exceeded and that the gas is released by a blistering mechanism.

The marked influence of damage on gas trapping is shown in Fig. 21, according to Ref. /62/. Profile studies of hydrogen trapping in molybdenum predamaged by helium, oxygen, neon and bismuth ions were performed by Picraux et al. /68/. For a given predamage dose, hydrogen retention increases linearly with hydrogen fluence until a saturation level is reached. Increased predamage fluence results in increased saturation level for hydrogen trapping as high as 10 at.% achieved. An ion-mass dependence indicates that the lighter ions, which create fewer primary displacements, are more effective in hydrogen trapping, suggesting a lower efficiency of the denser cascades of heavier ions in forming the defect types needed in hydrogen trapping.

There is another way in which hydrogen ion trapping occurs. In certain metals hydrogen reacts chemically and has a large positive heat of solution, e.g. titanium, zirconium, niobium, tantalum and the rare earths /69/. Thus, implanted hydrogen ions can diffuse into the bulk of the metal without being able to penetrate the potential barrier at the surface. For example, in titanium a hydride surface layer is formed at intermediate temperatures. At higher temperatures, however, no evidence of TiH is found indicating that the hydrogen must be diffusing into the bulk of the specimen. Surface deformation is again found at low temperatures.

#### 4.2 The formation and behaviour of gas bubbles in the bulk

The earliest systematic studies of bubble behaviour were done in uranium or plutonium based fuels containing about 10 % fission gases, such as krypton and xenon, after neutron irradiation /70, 71/. Bubbles containing helium gas became interesting when high-temperature embrittlement in fuel claddings was observed and attributed to helium /7/. The recent interest in helium gas bubbles is channeled in the CTR research program. Nearly all studies are therefore concentrated on potential structural materials in a CTR environment, for example, aluminium /72/, stainless steel /73/ and the refractory materials vanadium /74/, molybdenum /74/, niobium /75/ and their alloys. The evidence of bubbles is usually studied by means of transmission-electron-microscopy (TEM) techniques, but some efforts have been made to trace the evolution of bubbles by means of positron annihilation /76/, where the substitutional helium is found to be a trapping site for positrons. In the

absence of intense 14 MeV neutron sources the irradiations are performed by implanting helium into the metal in order to simulate the damage caused by free alpha particles from the (d,t) reaction.

Detailed studies on helium bubble formation covering the whole implantation depth are reported by Kaletta /12/ for 200- and 2000 KeV helium ions in vanadium. The temperature range chosen from 700 to 1000 K ( $0.3 - 0.6 T_m$ ) allows vacancy migration and ensures supersaturation of free vacancies during irradiation. Three different modes of bubble growth could be established exhibiting a pronounced dependence on temperature, dose and penetration depth as schematically illustrated in Fig. 22.

- (1) At low temperatures ( $< 800$  K) and low dose ( $< 10^{16}/\text{cm}^2$ ) no bubble occurred in the damage and helium peak region, but far beyond the peaks bubbles were found. Since at these temperatures and doses, no significant helium release is observed and the theoretical helium profile fits that monitored by nuclear reaction techniques /60, 77/, the onset of bubble growth beyond the peak was attributed to a stress-induced growth of helium-rich clusters. Recently for bubbles of low diameters ( $D < 1$  nm) Baskes and Holbrook /84/ published pressure curves as a function of helium density for various numbers of vacancies based on an isotropic linear elasticity theory. They found that helium atoms put into vacancies in copper produce a volume increase of about 0.62 atomic volumes per helium atom, when the number of helium atoms is larger than the number of vacancies. The pressures due to the gas-metal interactions are extremely high, between 100 and 200 GPA. The internal pressure required for the ejection of an interstitial is of the order of 35 GPA, if the formation energy is about 3.5 eV in Copper /85/. Thus, a pressure-induced growth cannot be excluded, though the calculations by Baskes and Holbrook are just valid for zero-point considerations. At higher temperatures the internal pressures are probably lower by more than one order of magnitude. Due to the high pressures needed for pushing an interstitial into the lattice, this process operates possibly in the nucleation phase rather than in the growth phase. A different mechanism for strain relief of overpressurized bubbles had been considered by Greenwood et al. /38/. Bubbles can expand by punching out interstitial loops as sketched in Fig. 23. By considering the energies involved Greenwood et al. showed that the reaction would occur at lower gas

pressures decreasing with increasing bubble radius according to  $\mu b/r$  where  $\mu$  is the shear modulus of the material and  $b$  is the Burgers-vector. For example, the pressure for loop-punching is about 5 GPA for a bubble of 1 nm radius.

- (2) The increase in temperature or in dose enhancing diffusion by offering more free vacancies enforces bubble growth and bubbles are now observed along the penetration depth and, again, far beyond. The increase in bubble concentration and diameter with temperature and dose indicates a permanent nucleation and growth, but whether this is by continued arrival of helium at bubble surfaces followed by vacancy absorption, in order to reach thermal equilibrium or by predominant vacancy absorption (or both) cannot be said. Simple calculations for a gas-driven growth-rate support a growth behaviour controlled by the arrival of gas atoms /12/.
  
- (3) At about  $0.4 T_m$ , where bubble swelling in vanadium is at a maximum, a third growth mode could be identified in the peak region: the coalescence of bubbles. With increasing dose the bubble concentration declines which is accompanied by an strong increase in bubble diameter. From the diameter-vs.-dose curve a fourth order power law dependence could be determined excluding the possibility of growth due to Oswald ripening. For this process A.J. Markworth predicted a quadratic dependence /78/. At high temperatures coalescence is favoured by pairwise agglomeration of bubbles of the same diameters on the average /40/, as shown in table 4, where the bubble diameters observed and calculated are compared on the basis of a van-de-Waals law for 240 KeV helium in vanadium. From these data the activation energy could easily be ascertained to 1.13 eV if volume diffusion was assumed, and to 0.83 eV for surface diffusion /12/. These values are considerably lower than that of 2.6 eV calculated by Smidt and Pieper /79/ on the base of the Gruber model /80/ from thermal annealing experiments. At temperatures around  $0.4 T_m$  the coalescence process is found to be complex and pairwise agglomeration of bubbles of the same average diameters cannot be found /12/.

The dose dependence of bubble growth for different CTR-parameters in vanadium is summarized in Fig. 24, according to Ref. /57/. A linear behaviour is only found up to several thousand appm helium implanted. Thereafter a oscillating behaviour is indicated (clearly seen in the case of the lower CTR-parameter) representing the change in the growth modes discussed above.

The most interesting feature, however, was found by counting the number of helium atoms in gas bubbles. Assuming thermal equilibrium which seemingly holds for large bubbles above  $0.4 T_m$  /40/, the gas pressure represented by a van-de-Waals law is balanced by the surface pressure  $2\gamma/r$ . Thus the gas atom number,  $m$ , is neglecting the correction for the intermolecular forces:

$$m = \frac{8\pi r^2}{3(kT+2B\gamma/r)} \quad (4)$$

$k$  = Boltzmann-Konstante  
 $T$  = Temperature  
 $B$  = van de Waals constant  
 $\gamma$  = surface energy  
 $r$  = bubble radius

Based on this equation, Chen and Cost /81/ found that the helium count in bubbles after cyclotron injection with alpha particles in aluminium followed by heat treatment is higher by roughly a factor of three than the amount injected. In a similar experiment in stainless steel. Smidt and Pieper /73/ found that the calculated helium concentration from TEM micrographs increases to the amount injected with increasing annealing temperature. The current concept that all helium implanted is collected in bubbles is also supported by low-dose experiments in vanadium. But by increasing the dose a large discrepancy between the amount of helium calculated and that implanted was found by Kaletta /40/, as is shown in Fig. 25. The bubbles taken into account in the calculation were large, well resolved cavities with mean diameters of more than 10 nm. We assumed a van-de-Waals law and thermal equilibrium conditions for bubbles using a surface energy of 1 N/m. Corrections of the surface energy (up to 2 N/m) and to non-thermal bubble conditions (gas excess pressures as high as the yield strength, up to  $2 \text{ kN/m}^2$ ) increased the amount of helium collected in bubbles in each case by a factor of less than 1.5. The same factor was found when the van-de-Waals constant  $B$  was replaced by the temperature-dependent second virial coefficient as given by Tseiderberg et al. /83/. The maximum experimental

error is about 50 % as indicated in Fig. 24 for one point. The magnitude of these corrections is in agreement with a paper recently published by Cost and Chen /83/ discussing the compressibility behaviour and the surface energy corrections in more detail. Large corrections by an order of magnitude were found for small bubble radii ( $1 < R < \text{nm}$ ) and corrections by a factor of less than 2 for large bubbles ( $R > 10 \text{ nm}$ ). They conclude that the best method of characterizing the compressibility behaviour of the gas phase is to use the virial equation and the temperature-dependent second and third virial coefficients as published by Tseiderberg et al. but in no case can the large discrepancy seen in Fig. 24 for high doses be explained by correcting the gas law, if the bubbles are large.

Thus, the question is: what has happened to the helium unobserved? Since there is not gas release at these temperatures and doses /60, 77/ it is assumed that (I) most of the helium implanted is collected in bubble bands at the grain boundaries which become more important at higher doses and/or (II) most of the helium is collected in small clusters of about 1 nm size which are growth-inhibited due to the lack of free vacancies which are absorbed by coalesced bubbles in order to relax. The estimated relaxation time is in the microsecond range at temperatures above 0.4 Tm

The first assumption could not be checked carefully, since no single bubbles in the bubble bands were resolved. The second assumption was studied in of annealing experiments to establish the development of a new bubble population annealing at low diameters /86/. Vanadium samples prior irradiated and analyzed by TEM techniques were annealed and again analyzed by TEM methods. After annealing a second peak indicated at low diameters is more pronounced than the peak at higher diameters of the as-irradiated samples, as shown in Fig. 26. The bimodal structure of the population curve was attributed to bubbles grown by absorbing either irradiation-induced vacancies or thermally created vacancies. The net effect on the helium gain is small, however, and just 10 % helium is additively found after annealing.

No differences are reported by G. Fenske et al. /87/ who irradiated either 20- or 500 KeV helium ions in nickel to total doses of 3 and  $5 \times 10^{17} \text{ cm}^{-2}$ , respectively. The bubble concentrations they measured are about an order of magnitude higher (up to  $10^{17} / \text{cm}^3$ ) than those reported for vanadium and no

bubbles are found far beyond the mean penetration depth. In the light of the theoretical calculations by Wilson and Johnson /51/ these results are unexpected, since helium in nickel shows a similar behaviour as helium in vanadium (extremely low interstitial migration energy, high interstitial formation energy) which is in contrast to the behaviour of helium in most of the F.C.C. metals.

Above a dose of  $1 \times 10^{17}/\text{cm}^2$ , Evans and coworkers /74/ in molybdenum observed a high density of small bubbles aligned approximately on a B.C.C. superlattice as seen in Fig. 27. The  $[110]$  bubble spacing of about 3.5 nm is relatively insensitive to variations of the temperature ranging from 300 up to 1000 K (0.1 - 0.34 Tm), the ion energy ranging from 36 to 100 KeV and the ion dose ranging from 1 to  $8 \times 10^{17}/\text{cm}^2$ . There is not sign of large bubbles such as those towards the end of the helium range in vanadium. Data from high-temperature irradiations of 0.42 Tm in molybdenum support the large bubble formation exhibiting a overall structural complexity which consists of a coarse distribution of large clearly delineated thin areas and a finer distribution of much smaller helium bubbles widely varying in size between 5 and 100 nm /74/.

The dependence of bubble formation on ion energy has not yet been studied in detail. Results comparing 200 and 2000 helium irradiations in vanadium /12/ indicate differences in bubble size and concentration. In the case of higher energy larger bubbles (up to several 100 nm) are found, whereas the concentrations are going down by an order of magnitude. These scaling effects were attributed to an enhanced coalescence process, but it is not clear, whether the process is really enhanced due to the increased displacement damage (by about 20 %) in the case of the higher ion energy or whether it has proceeded due to an increased irradiation time, since the flux decreased by a factor of 4. A pronounced flux-dependence caused by the different times for reaching a given dose level has been observed in vanadium after 200 KeV helium irradiation as is shown in Fig. 28, according to Ref. /12/.

The effects on bubble growth in vanadium of coupled thermally created and irradiation induced vacancies have recently been published /88/. In beam-cycling experiments the samples received their total doses in a number of shots. Between these shots the temperature was held at the same value as

that during the implantation. The significant feature was a saturation effect after a few cycles the dominant growth process during cycling, the coalescence of bubbles, came to rest after the bubbles become too large to be mobile, as is seen in Fig. 29, according to Ref. /88/.

#### 4.3 The surface bubbles - blistering, exfoliation and perforation

In the early sixties Primak /89/ and Kaminsky /90/ first reported experimental evidence for blister formation in insulators irradiated with 100 - 140 KeV protons and helium ions and in metals with 125 KeV deuterons, respectively. Due to its potentially serious implications in fusion reactor technology /91, 92/ the blistering phenomenon grew in importance and has been the subject of many experiments. Two sets of conditions have to be fulfilled for the appearance of blistering.

(1)

The depth  $x$ , at which the ions come to rest must be larger than the thickness sputtered away at a critical dose  $D_c$  requiring for blister formation /62, 93/. If  $S$  is the sputtering yield and  $n$  the atomic density of the material this means, that  $S < xn/D_c$ . In the case of light ions such as hydrogen or helium the condition holds for all energies. For heavy ions such as argon blistering can occur only at energies above 100 KeV when the sputtering yield decreases. The critical dose is related to a critical pressure  $p_c$  to deform the surface and it can be written as

$$p_c = \frac{4\sigma t^2}{r^2} \quad \begin{array}{l} \sigma = \text{yield strength} \\ t = \text{thickness of blisterskin} \\ r = \text{blister radius} \end{array} \quad (5)$$

Although some general trends support this equation, a specific behaviour cannot be predicted on the base of this equation. For example, there is a smooth temperature dependence of the blister dose decreasing with increasing temperature /95/ which is attributed to the decrease in the yield strength with increasing temperature on the other hand the increase of yield strength by alloying pure vanadium with 3 % titanium (solid solution) reduces the

critical dose due to microstructural effects associated with an altered ratio of grain boundary to matrix strength /40/. This agrees with a similar experiment of Das and Kaminsky /94/ who had found an influence of the initial dislocation density on the critical dose reduced by a factor of two. The increase in the critical dose is again in accordance with the equation given above. For gases such as hydrogen which have a high permeability in metals  $D_c$  is generally higher than for inert gases such as helium as reported by Kaminsky and Das /95/.

(2)

Solubility and diffusivity of the implanted ion in metals are the second set of conditions affecting the blistering process. Blister formation can only occur when the temperature is low enough to ensure gas-trapping and when the solution limit is exceeded to build-up the critical pressure needed for surface deformation. In accordance to the different behaviour of hydrogen and helium in metals discussed in Sect. 4.1, differences in blistering behaviour have been observed by many authors /60, 95, 96/.

Qualitative models for the formation of blisters have been suggested by a number of authors. These fall into two major categories: the first category will be called the gas-driven model based on the formation of small gas bubbles and the second category considers mainly the stresses in the implanted layer and will be called the stress model.

Primarily the gas-driven models are developed to explain blistering at low temperatures, below  $0.3 T_m$ , where the vacancy mobility is negligible. The formation of surface blistering on metals is explained /97/ by the athermal coalescence of small (1 - 2 nm diameter) helium equilibrium bubbles, the condition for coalescence being satisfied when the bubbles are large enough to touch. Since the bubbles cannot grow by vacancy absorption at low temperatures, a critical density of these small bubbles is required above coalescence is initiated. Evans /98/ has suggested that the coalescence of bubbles becomes very rapid when the volume swelling due to the gas bubbles in the implant region reaches a critical value. Thus, the critical dose for blister appearance is governed by a critical value of volume swelling being estimated to about 50 % which is in agreement with available critical dose values in niobium and molybdenum irradiated with helium ions of different

energies (30 - 300 KeV). The coalescence, once started becomes a run-away process and an unstable high pressure cavity easily can form which leads to the plastic deformation of the surface layer. According to equations (4) and (5) the critical gas pressure in large cavities (0.1 micron) is higher than the gas pressure in a cavity of same size being in thermal equilibrium. Thus, a cavity with a radius of 0.1 micron will not form a blister unless further coalescence occurs leading to the excess internal bubble pressure at constant bubble volumen. In those cases, where the coalescence extends very rapidly due to an increased target-temperature up to about  $0.3 T_m$  to give cavity diameter much larger than needed for plastic deformation, the excess pressure can build up to much higher values and the blister skin can readily rupture. In the case that blisters reach the dimension of the grains, exfoliation of grain areas or even across the entire implant area crossing numerous grain boundaries occurs characteristic for the second mode of surface deformation.

It was shown by in-situ observations /99/ that exfoliation proceeds with increase in total dose and peeling of successive layers at multiples of the critical dose takes place which is in contrast to blistering. The blisters one formed rapidly at the critical dose cover the sample surface uniformly. Further implantations as much as an order of magnitude greater than the critical dose did not produce additional blistering. The flaking of the surface during irradiation is accompanied by bursts in the reemission rate as seen in Fig. 20, Whilst exfoliation in titanium is significantly reduced by cold-working /99/, exfoliation in vanadium is observable up to  $0.5 T_m$  by alloying with titanium and hence increasing yield-strength as shown in Fig. 30.

At high target temperatures the build-up of internal pressure could be prevented by the presence of thermal vacancies leading to a permanent growth of bubbles until they are able to cut the surface. The performance - the third mode of surface deformation - is characterized by a steep rise in the reemission rate to values of nearly 100 % of incident flux Fig. 20.

The intuitive view of the coalescence model that the action of blister formation must be initiated at the depth of helium peak concentration has been shaken by the experimental results obtained recently by the Garching group /93, 100, 101/ which show that values of blister lid thickness

("Deckeldicke") to be appreciably larger than the depth for helium ion energies below 100 KeV. To overcome this difficulty, Evans /102, 103/ developed a model in which a blister is nucleated by the interbubble fracture of highly overpressurized helium bubbles. These bubbles are present around the peak at lower temperatures and beyond the peak at intermediate temperatures. In an initial phase their growth is controlled by a loop punching mechanism, but with increasing bubble size their growth is governed by an interbubble fracture mechanism schematically outlined in Fig. 31 according to Ref. /102/. At some critical depth from the incident surface a layer of bubbles may have sufficient pressure to coalesce by interbubble fracture and create an internal crack. If the pressure difference between the gas in the crack and the gas in the bubbles adjacent to the crack is sufficient a process of "unzipping" layers of bubbles can take place being able to start deformation the layer of material above the crack to give the final blister cross-section.

The principal feature of the interbubble fracture model, namely, that the blister lid deformation is totally gas-driven is supported by an experiment reported recently by Evans /104/. In this experiment a wedge-shaped molybdenum target bombarded with 100 KeV helium ions shows blister production on both the compression and tension surface of the thin foil target.

The interfracture model is developed to explain especially the experimental results in molybdenum studied by Evans intensively. It does not hold in cases, where the presence of sufficient vacancies will tend to keep the helium bubbles in equilibrium and hence suppress the possibility of interbubble fracture. In the case of vanadium at temperatures about  $0.4 T_m$  the appearance of blister, however, is accompanied by large gas bubbles assumed to be in thermal equilibrium as demonstrated in Fig. 15. Furthermore, the Evans model cannot explain the relation between the most probable blister diameter,  $d$ , and the blister skin thickness,  $t$ , found to be proportional to  $d^{2/3}$  in niobium /100/. Recent experimental results of Das et al. /105/, however, do not confirm this relationship and the exponents found are 1.25, 0.85, 1.15 and 1.22 for Be, V, Ni and Nb targets, respectively, bombarded with helium ions in the energy range 20 to 500 KeV.

Another model of helium clustering leading to blister deformation has been considered by Thomas and Bauer /106/ and Wilson et al. /107/ using percolation theory. According to this model the critical dose for blister appearance is the dose at which the concentration of helium reaches the value for the onset of percolation, i.e. helium atoms become connected to each other and hence mobile along this infinitely connected chain. Wilson et al. calculated the onset for B.C.C. metals at an atom fraction of 0.243 and for F.C.C. metals at an atom fraction of 0.199. The fact that the majority of implanted helium is in form of bubbles at high doses does not enter into this model directly.

More recently Behrisch et al. /101/ and Roth et al. /100/ have suggested that for low-energy helium ion irradiation of niobium the blister formation may be due not to the high gas-pressure but to the stress induced in the implanted layer. The stresses are assumed to be proportional to the bubble volume swelling found to be at the maximum at the end of the range of ions at certain temperatures /12/. Applied to the experimental results in niobium, the stress model /108/ can explain (I) the large blister skin thickness being thicker than the mean penetration depth and (II) the diameter-thickness relation quoted above.

Another area of experimental interest concerns the conditions governing whether blisters are found or whether exfoliation takes place after helium bombardment. In a recent paper, Risch /109/ concludes that exfoliation is affected by temperature, where the important parameter is the gas pressure rather than the lateral stress that He proposes at lower temperature for the blister onset.

The stress model, however, cannot explain the absence of blistering in analogous ion-beam studies involving void-swelling, where the stress systems should be similar. In cases of large void-swelling Johnston et al. /110/ could show that the ingrated swelling is totally reflected in the step height between bombarded and shielded regions.

## References

- /1/ C. Cawthorne and J.E. Fulton, *Nature*, 216 (1956) 575
- /2/ B.L. Eyre, KfK Report 2590 (1978) 58
- /3/ D. Kaletta, KfK Report 2590 (1978) 32
- /4/ A.D. Brailsford and R. Bullough, *J. Nucl. Mater.*, 44 (1972) 121
- /5/ A.D. Marwick, *J. Nucl. Mater.*, 55 (1975) 259
- /6/ D.M. Parkin and A.N. Goland, *Proc. Intern. Conf. Radiation Effects and Tritium Technology and for Fusion Reactors, Gatlinburg, TN (USA), Oct. 1975, Vol. 1, 417*
- /7/ D.R. Harries, *J. Brit. En. Soc.*, 1966, p. 74
- /8/ *Proc. Intern. Conf. Effects of Hydrogen on the Behaviour of Materials, Jackson, Wyoming (USA), Sept. 1975*
- /9/ G.L. Kulcinski, see Ref. /6/, Vol. 1, 17
- /10/ H. Wiedersich, J.J. Burton and J.L. Katz, *J. Nucl. Mater.* 51 (1974) 287
- /11/ I. Manning and G.P. Mueller, *Comp. Phys. Comm.* 7 (1974) 85
- /12/ D. Kaletta, KfK Report 2282 (1976)
- /13/ M.R. Hayns, M.H. Wood and R. Bullough, *J. Nucl. Mater.* 75 (1978) 241
- /14/ G.R. Odette and S.C. Langley, s. Ref./6/, Vol. 1 395
- /15/ R. Bullough and R.C. Perrin, *Proc. Intern. Conf. Radiation Damage in Reactor Materials, Vienna (A), June 1969, Vol. II, 233*
- /16/ H. Wiedersich, *Radiat. Eff.* 12 (1972) 111
- /17/ S.J. Rothmann, N.Q. Lam, R. Sizmann and H. Bisswanger, *Radiat. Eff.* 20 (1973) 223
- /18/ A.J.E. Foreman, *Radiat. Eff.* 21 (1974) 81
- /19/ J. Bressers and M. Cambini, *J. Nucl. Mater.* 68 (1977) 250
- /20/ W. Schilling and K. Schröder, *AERE Report 7934 (1974) 212*
- /21/ G. Dünsing, H. Hammerich, W. Sassin and W. Schilling, *Proc. Intern. Conf. Vacancies and Interstitials in Metals, Jülich (D) Sept. 1968*
- /22/ A. Seeger, D. Schuhmacher, W. Schilling and J. Diehl (Editors), *Vacancies and Interstitials, Amsterdam 1970 (North-Holland Publ. Comp.)*
- /23/ M.T. Robinson and F.W. Young (Editors), *Proc. Intern. Conf. Fundamental Aspects of Radiation Damage in Metals, Gatlinburg, TN (USA), Oct. 1975*
- /24/ J.A. Brinkmann, *J. Appl. Phys.* 25 (1954) 961
- /25/ A. Seeger, *Proc. 2nd Intern. Conf. on Peaceful Uses of Atomic Energy, Geneva (CH) 1958, Vol. 6, 250*
- /26/ C.A. English, *Application of Ion Beams to Materials 1975, Inst. Phys. Conf. Ser. 28 (1976) 257*
- /27/ M.L. Jenkins, K.H. Katerbau and M. Wilkens, *Phil. Mag.* 34 (1976) 1141 (Part I) M.L. Jenkins and M. Wilkens, *Phil. Mag.* 34 (1976) 1155 (Part II)
- /28/ K. Winterbon, P. Sigmund and J.B. Sanders, *Mat. Fys. Medd. Van. Vid. Selsk.* 14 (1970)

- /29/ R. Bullough, K. Krishan and B.L. Eyre, AERE Report 7952 (1975)
- /30/ P.T. Heald and M.V. Speight, J. Nucl. Mater. 64 (1977) 139
- /31/ W. Primak and J. Luthra, J. Appl. Phys. 37 (1966) 2287
- /32/ R. Syre, AD Report 476420 (1965)
- /33/ C. Cawthorne, E.J. Fulton, J.I. Bramman, G.A.B. Linekar and R.M. Sharpe, Proc. BNES Conf. Voids Formed by Irradiation of Reactor Materials, Reading (GB) 1971, p. 35
- /34/ P.J. Burton, B.L. Eyre and D.A. Stow, J. Nucl. Mater. 67 (1977) 181
- /35/ D. Kaletta and W. Schneider, KfK Report 1652 (1972)
- /36/ K. Ehrlich and R. Gross, IAEA Symp. Fuel and Fuel Elements for Fast Reactors, Brussels (B), July 1973, Vol. II, 179
- /37/ R.S. Barnes, J. Nucl. Mater. 11 (1964) 135
- /38/ G.W. Greenwood, A.J.E. Foreman and D.E. Rimmer, J. Nucl. Mater 4 (1959) 305
- /39/ K. Ehrlich and D. Kaletta, s. Ref. /6/, Vol. II, 289
- /40/ D. Kaletta, J. Nucl. Mat. 63 (1976) 347
- /40.1/W. Bauer and G.J. Thomas, Nucl. Metallurgy 18 (1973) 255
- /40.2/R.S. Nelson, J.A. Hudson and D.J. Mazey, AERE Report 7120 (1972)
- /40.3/W.V. Vaidya, KfK Report 2567 (1977)
- /41/ D.J. Reed, Radiat. Eff. 31 (1977) 129
- /42/ R.A. Johnson, Phys. Rev. 145 (1966) 423
- /43/ D.E. Rimmer and A.H. Cottrell, Phil. Mag. 2 (1957) 1345
- /44/ R.A. Johnson, Phys. Rev. 152 (1966) 629
- /45/ W.D. Wilson and C.L. Bisson, Phys. Rev. B3 (1971) 3984
- /46/ D.E. Harrison, G.L. Vine, J.A. Tankovich and R.S. Williams, Proc. Intern. Conf. Applications of Ion Beams to Metals, Albuquerque, NM (USA), Oct. 1973, p. 227
- /47/ W.D. Wilson and C.L. Bisson, Radiat. Eff. 22 (1974) 63
- /48/ W.D. Wilson, M.I. Baskes and C.L. Bisson, Phys. Rev. B13 (1976) 2470
- /49/ L.M. Caspers, H. van Damm and A. van Veen, Delft Prog. Rep. Ser. A1 (1976) 39
- /50/ W.D. Wilson and C.L. Bisson, Radiat. Eff. 25 (1975) 197
- /51/ W.D. Wilson and J.A. Johnson, Interatomic Potentials and Simulation of Lattice Defects, ed. by P.C. Gehlen, J.R. Beeler and R.I. Jaffee, New York 1972 (Plenum Press), p. 375
- /52/ J. Th. M. DeHosson, A.W. Sleswyk, L.M. Caspers, W. van Hengen and A. van Veen, Solid State Comm. 18 (1976) 479
- /53/ W.D. Wilson and C.L. Bisson, Bull. Am Phys. Soc. 19 (1974) 372
- /54/ M.W. Guinan and R.M. Stuart, ANS Transactions 21 (1975) 164
- /55/ M.I. Baskes and W.D. Wilson, J. Nucl. Mater. 63 (1976) 126
- /56/ R.S. Blewer, s. Ref. /46/, p. 557

- /57/ D. Kaletta, Proc. Reaktortagung 1978, Hannover (D), April 1978, p. 1017
- /58/ E.V. Kornelson, Radiat. Eff. 18 (1972) 227
- /59/ G.J. Thomas and W. Bauer, s. Ref. /46/, p. 533
- /59.1/ J. Roth, S.T. Picraux, W. Eckstein, J. Bottiger and R. Behrisch, s. Ref. /87/
- /60/ W. Bauer and G.J. Thomas, J. Nucl. Mater. 53 (1974) 127
- /60.1/ G.J. Thomas and W. Bauer, J. Nucl. Mater. 53 (1974) 134
- /61/ W. Bauer and G.J. Thomas, J. Nucl. Mater. 63 (1976) 299
- /62/ S.K. Erents and G.M. McCracken, Radiat. Eff. 18 (1973) 191
- /63/ K.D. Wilson and G.J. Thomas, J. Nucl. Mater. 63 (1976) 266
- /64/ S.K. Erents and G.M. McCracken, J. Phys. D2 (1969) 1397
- /65/ S.K. Erents and G.M. McCracken, Radiat. Eff. 3 (1970) 123
- /66/ T. Picraux and F.L. Vook, s. Ref. /46/, p. 407
- /67/ K.L. Wilson, G.J. Thomas and W. Bauer, Nucl. Technology, 29 (1976) 322
- /68/ S.T. Picraux, J. Bottiger and N. Rud, Appl. Phys. Lett., 28 (1976) 179
- /69/ G.M. McCracken, D.K. Jefferies and P. Goldsmith, Inst. Phys. Conf.
- /70/ B.L. Eyre and R. Bullough, J. Nucl. Mater. 26 (1976) 249
- /71/ M.E. Gulden, J. Nucl. Mater. 23 (1967) 30
- /72/ E. Rüdél, O. Gautsch and E. Staroste, J. Nucl. Mater. 62 (1976) 63
- /73/ F.A. Smidt, Jr. and A.G. Pieper, s. Ref. /23/, Vol. II, 250
- /74/ J.H. Evans, D.J. Mazey, B.L. Eyre, S.K. Erents and G.M. McCracken, s. Ref. /26/, p. 299
- /75/ A.A. Sagues and J. Auer, s. Ref. /23/, Vol. II, 331
- /76/ C.L. Snead, Jr. A.N. Goland and F.W. Wiffen, J. Nucl. Mater. 64 (1977) 195 Ser., 5 (1968) 149
- /77/ R.S. Blewer and R.A. Langley, J. Nucl. Mater. 63 (1976) 337
- /78/ A.J. Markworth, Met. Trans. 4 (1973) 2651
- /79/ F.A. Smidt, Jr. and A.C. Pieper, J. Nucl. Mater. 51 (1974) 361
- /80/ E.E. Gruber, J. Appl. Phys. 38 (1967) 243
- /81/ K.Y. Chen and J.R. Cost, J. Nucl. Mater. 52 (1974) 59
- /82/ J.R. Cost and K.Y. Chen, J. Nucl. Mater. 67 (1977) 265
- /83/ N.V. Tsederberg, V.N. Popov and N.A. Morozova, Thermodynamic and Thermophysical Properties of Helium (Translated from Russian in: Translation TT70-50096, 1971, US depart. of Commerce, Nat. Techn. Inform. Office, Wash., D.C.)
- /84/ M.I. Baskes and J.H. Holbrook, Phys. Rev. B17 (1978) 422
- /85/ R.A. Johnson and W.D. Wilson, s. Ref. /51/, p. 301
- /86/ D. Kaletta and J.F. Stubbins, J. Nucl. Mater. 74 (1978) 93
- /87/ G. Fenske, S.K. Das, M. Kaminsky and G.H. Miley, Proc. 3rd Intern. Conf. Plasma Surface Interactions in Controlled Fusion Devices, Culham (GB), April 1978

- /88/ D. Kaletta, J. Nucl. Mater. 76 (1978) 221
- /89/ W. Primak, J. Appl. Phys. 34 (1963) 3630
- /90/ M. Kaminsky, Adv. in Mass Spectrometry 3 (1964) 69
- /91/ M. Kaminsky, Proc. Int. Working Session on Fusion Reactor Technology, Oak Ridge, 1971, IEEE Trans. Nucl. Sci. 18 (1971) 208
- /92/ R. Behrisch, Nucl. Fusion 12 (1973) 695
- /93/ J. Roth, R. Behrisch and B.M.U. Scherzer, J. Nucl. Mater. 53 (1974) 147
- /94/ S.K. Das and M. Kaminsky, J. Appl. Phys. 44 (1973) 44
- /95/ M. Kaminsky and S.K. Das, Radiat. Eff. 18 (1973) 245
- /96/ H. Verbeek and W. Eckstein, s. Ref. /46/, p. 597
- /97/ J.H. Evans, J. Nucl. Mater. 61 (1976) 1
- /98/ J.H. Evans, Nature 256 (1975) 299
- /99/ G.J. Thomas and W. Bauer, J. Nucl. Mater. 63 (1976) 280
- /100/ J. Roth, Inst. Phys. Conf. Ser. 28 (1976) 280
- /101/ R. Behrisch, J. Bottiger, W. Eckstein, U. Littmark, J. Roth and B.M.U. Scherzer, Appl. Phys. Letters 27 (1975) 199
- /102/ J.H. Evans, J. Nucl. Mater. 68 (1977) 129
- /103/ J.H. Evans, s. Ref. /87/
- /104/ J.H. Evans, J. Nucl. Mater. 67 (1977) 307
- /105/ S.K. Das, M. Kaminsky and G. Fenske, s. Ref. /87/
- /106/ G.J. Thomas and W. Bauer, Radiat. Eff. 17 (1973) 221
- /107/ W.D. Wilson, C.L. Bisson and D.E. Amos, J. Nucl. Mater. 53 (1974) 154
- /108/ E.P. Eernisse and S.T. Picraux, J. Appl. Phys. 48 (1977) 9  
Erratum 48 (1977) 2648
- /109/ M. Risch, IPP Report 9/24 (1978)
- /110/ W.G. Johnston and J.H. Rosolowski, Inst. Phys. Conf. Ser. 28 (1976)  
228

TABLES:

- Table 1 Binding energies in eV of the  $i^{\text{th}}$  vacancy and the  $j^{\text{th}}$  helium atom in a cluster (i, j) containing i vacancies and j helium atoms in copper (after Wilson, Bisson and Baskes 1976).
- Table 2 Migration energies  $E_m$  of clusters(g, v) in tungsten containing g helium atoms and v vacancies (after Caspers et al. 1976 and Wilson et al. 1972).
- Table 3 Comparison of the experimental and calculated bubble diameter in vanadium after 240 keV helium implantation at 973 K. Sample depth 0.8  $\mu\text{m}$ , surface energy 1 N/m. (After Kaletta, 1976).

## Figure Captions

- Fig. 1 The gas rate,  $K_g$ , and the displacement rate,  $K_v$ , in nickel for different irradiation sources at a flux of about  $10^{14}$  particles per  $\text{cm}^2$  and second.
- Fig. 2 Primary recoil spectra of different irradiation sources in niobium after Ref. /5/.
- Fig. 3 The specific damage energy in niobium as a function of the neutron energy after Ref. /6/.
- Fig. 4 The damage and helium distribution in vanadium implanted with helium ions at different energies as a function of the penetration depth after Ref. /12/.
- Fig. 5 the CTR-parameter in vanadium as a function of depth. Dotted line: thermally created displacements only.
- Fig. 6 Steady state vacancy concentration as a function of inverse temperature  $dn/dT =$  displacement rate,  $p =$  sink annihilation probability. After Ref. /16/.
- Fig. 7 The irradiation-induced vacancy and interstitial concentration in vanadium implanted with 240 keV helium ions as a function of depth after Ref. /12/.
- Fig. 8 Schematic representation of a depleted zone according to A. Seeger.
- Fig. 9 Schematic diagram of irradiation-induced defects and related damage in vanadium as a function of the CTR-parameter and the temperature;  $g =$  number of helium atoms,  $v =$  number of vacancies,  $d =$  diameter.
- Fig. 10 TEM micrograph of nickel implanted with helium ions at room-temperature after Ref. /35/.
- Fig. 11 SEM micrograph of vanadium implanted with 6 keV helium ions after Ref. /12/.

- Fig. 12 TEM micrograph of well aligned loops in nickel after 60 keV helium implantation at  $T = 673$  K to a fluence of  $2 \times 10^{16}/\text{cm}^2$  Ref. /35/.
- Fig. 13 TEM micrograph of voids in an austenitic steel after cyclotron bombardment with  $3 \times 10^{17}$  20 MeV carbon ions per  $\text{cm}^2$  after Ref. /36/ .
- Fig. 14 TEM micrograph of bubbles in vanadium after 240 keV helium implantation after Ref. /12/.
- Fig. 15 micrographs of a vanadium sample after implantation with  $2 \times 10^{17}$  He ions per  $\text{cm}^2$  at  $T = 973$  K. a) SEM micrograph showing dome-shaped blisters. b) TEM micrograph showing cubic bubbles Ref. /40/.
- Fig. 16 Total elongation of vanadium and two ternary alloys implanted with 104 MeV alpha particles as a function of the test-temperature after Ref. /39/.
- Fig. 17 SEM micrograph of vanadium implanted with 240 keV helium ions after Ref. /12/.
- Fig. 18 TEM micrographs of bubbles in V-20 Ti implanted with 240 keV helium ions after Ref. /39/.
- Fig. 19 Minimum energy configurations of from two to seven helium atoms in a single vacancy in copper. The vacancy is described by an empty cube after Ref. /48/.
- Fig. 20 Helium re-emission rates of aluminium implanted with 20 keV helium ions after Ref. /63/.
- Fig. 21 Gas release during 20 keV deuterium implantation of damaged and annealed molybdenum after Ref. /62/.
- Fig. 22 The three modes of bubble growth in vanadium implanted with 200 keV helium ions (schematically).

- Fig. 23 Mechanism of bubble growth by loop punching after Ref. /103/.
- Fig. 24 The bubble population in vanadium implanted with 200 keV helium as a function of the helium fluence and the CTR-parameter after Ref. /57/.
- Fig. 25 The helium concentration in pure vanadium as a function of temperature and dose. Solid line: amount of helium implanted calculated by means of range values. Dotted line: amount of helium bubbles collected in observable bubbles ( $d > 4$  nm) after Ref. /40/.
- Fig. 26 The bubble population in vanadium implanted with 210 keV helium ion a) as-irradiated, b) irradiated and post-annealed after Ref. /86/.
- Fig. 27 TEM micrograph illustrating the alignment of helium bubbles in Mo irradiated at 575 K with  $2.3 \times 10^{17}$  40 keV helium ions per  $\text{cm}^2$ . The orientation is close to  $\langle 001 \rangle$  after Ref. /74/.
- Fig. 28 TEM micrographs of vanadium samples implanted with 240 keV helium ions at different fluxes after ref. /12/.
- Fig. 29 bubble populations obtained from TEM micrographs. 2 MeV helium ions in vanadium,  $T = 848$  K, unit dose =  $93 \text{ C/m}^2$ , sample depth =  $5.0 \pm 0.1 \text{ }\mu\text{m}$  after Ref. /88/.
- Fig. 30 The transition from blistering to exfoliation by alloying pure vanadium with different amounts of titanium.
- Fig. 31 Interbubble fracture mechanism

Table I. a) Binding energies, in eV, of the  $i^{\text{th}}$  vacancy in a cluster,  $(i,j)$ , containing  $j$  helium atoms. The energies were calculated for "end points" only, the path of migration was not determined in each case.

Number of Vacancies	Number of Helium Atoms in the Cluster										
	0	1	2	3	4	5	6	7	8	9	10
2	.22	.22	1.27	1.79	1.79	2.04	2.08	2.58	3.19	3.66	4.31
3	.45	.45	.45	1.20	1.79	1.83	1.92	1.86	1.79	2.10	1.95
4	.58	.71	.71	.60	1.28	1.64	1.78	2.21	2.53	2.20	2.32

Table I b) Binding energies, in eV, of the  $j^{\text{th}}$  helium atom in a cluster, (i,j), where i is the number of vacancies in Cu. The energies were calculated for "end points" only, the path of migration was not determined in each case.

Number of Vacancies	Number of Helium Atoms in the Cluster									
	1	2	3	4	5	6	7	8	9	10
0	-	.08	.18	.08	.18	-.02	-	-	-	-
1	1.84	.79	.57	.66	.60	.86	.25	.24	.20	.20
2	1.84	1.84	1.09	.66	.85	.90	.75	.85	.67	.85
3	1.84	1.84	1.84	1.25	.89	.99	.69	.78	.98	.70
4	1.97	1.84	1.73	1.93	1.25	1.13	1.12	1.10	.65	.82

Dose [ $10^{16}$ He <sup>+</sup> /cm <sup>2</sup> ]	time [s]	bubble concentr. [ $10^{15}$ cm <sup>-3</sup> ]	bubble diameter (exp.) [Å]	bubble diameter (calc.) [Å]	number of He atoms	number of vac. required for relaxation
2	30	4.2	222	222.0	1 x 50520	
8	120	2.2	300	299.7	2 x 50520	190,730
20	300	1.1	412	407.8	4 x 50520	531,070

Tab. 2: Comparison of the experimental and calculated bubble diameter in V after 240-keV He<sup>+</sup> implantation at 700°C; sample depth 0.8 μm.

---

CLUSTER:	(1,0)	(0,1)	(0,2)	(0,3)	(1,1)	(1,1)*	(1,2)	(1,3)	(2,1)	(3,1)
$E_m$ [EV]:	0.29	1.45	1.6	1.4	5.07	4.75	1.6	1.4	>5.0	>5.0

---

\* = SUBSTITUTIONAL DE - TRAPPING

TABLE 3



MIGRATION ENERGIES  $E_m$  OF (g,v) - CLUSTERS IN TUNGSTEN g= NUMBER OF HELIUM ATOMS, v= NUMBER OF VACANCIES

DK 78 - 17

	FISSION NEUTRONS	FUSION NEUTRONS	HELIUM IONS (PEAK VALUES)
$K_g$ [GPA/S]	$10^{-13} - 10^{-12}$	$10^{-11}$	$10^{-4}$
$K_v$ [DPA/S]	$10^{-7} - 10^{-6}$	$10^{-6}$	$10^{-3}$

Fig. 1



HELIUM GENERATION RATE,  $k_g$ , AND THE DISPLACEMENT RATE,  $k_v$ , FOR DIFFERENT IRRADIATION SOURCES AT A FLUX OF  $10^{14}$  PARTICLES PER  $\text{cm}^2$  AND SECOND.

D. KALETTA  
DK 78-16

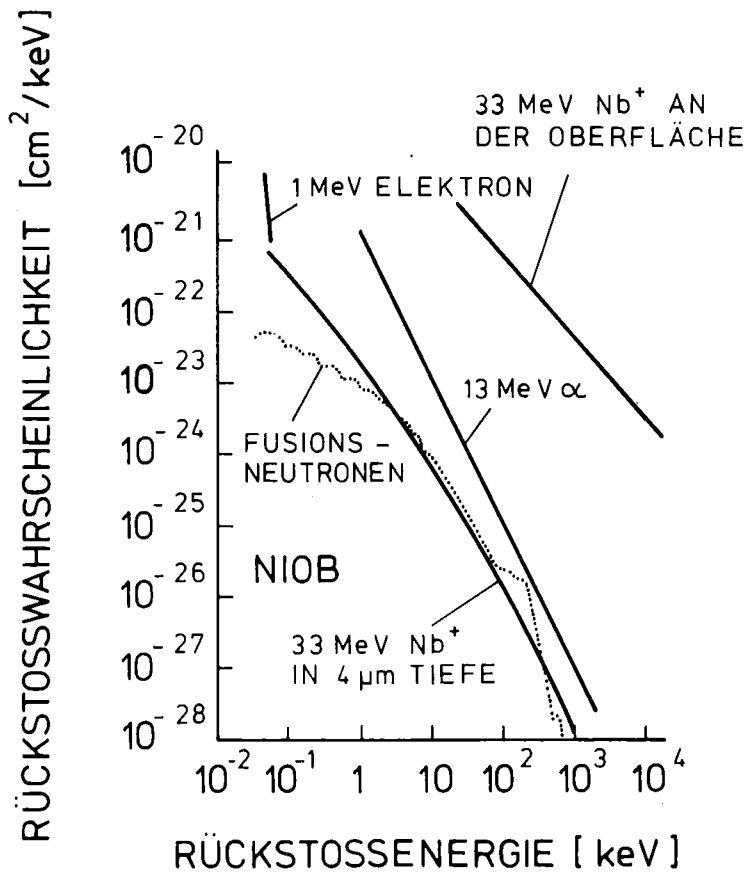


Fig. 2

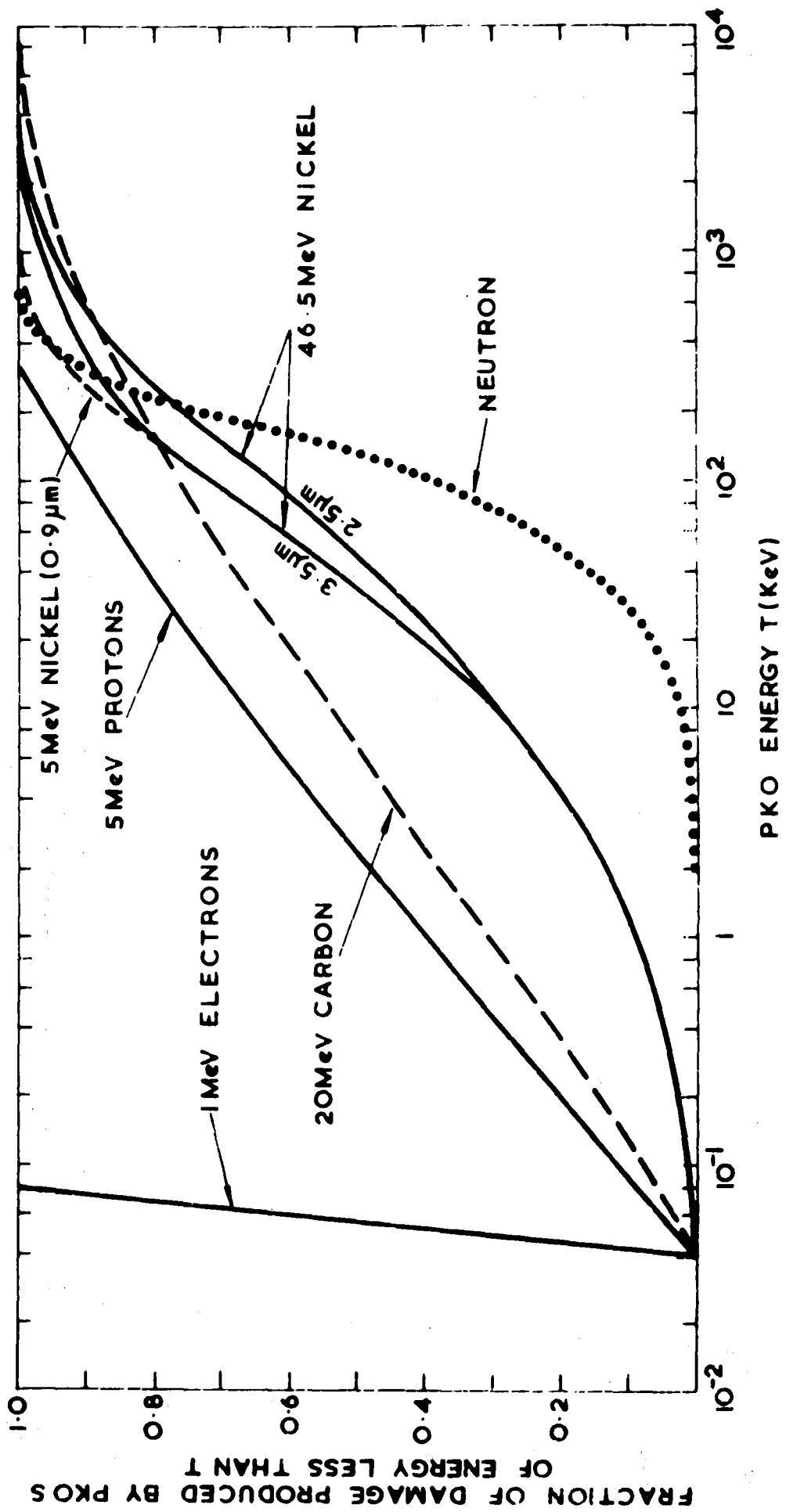


Fig. 3

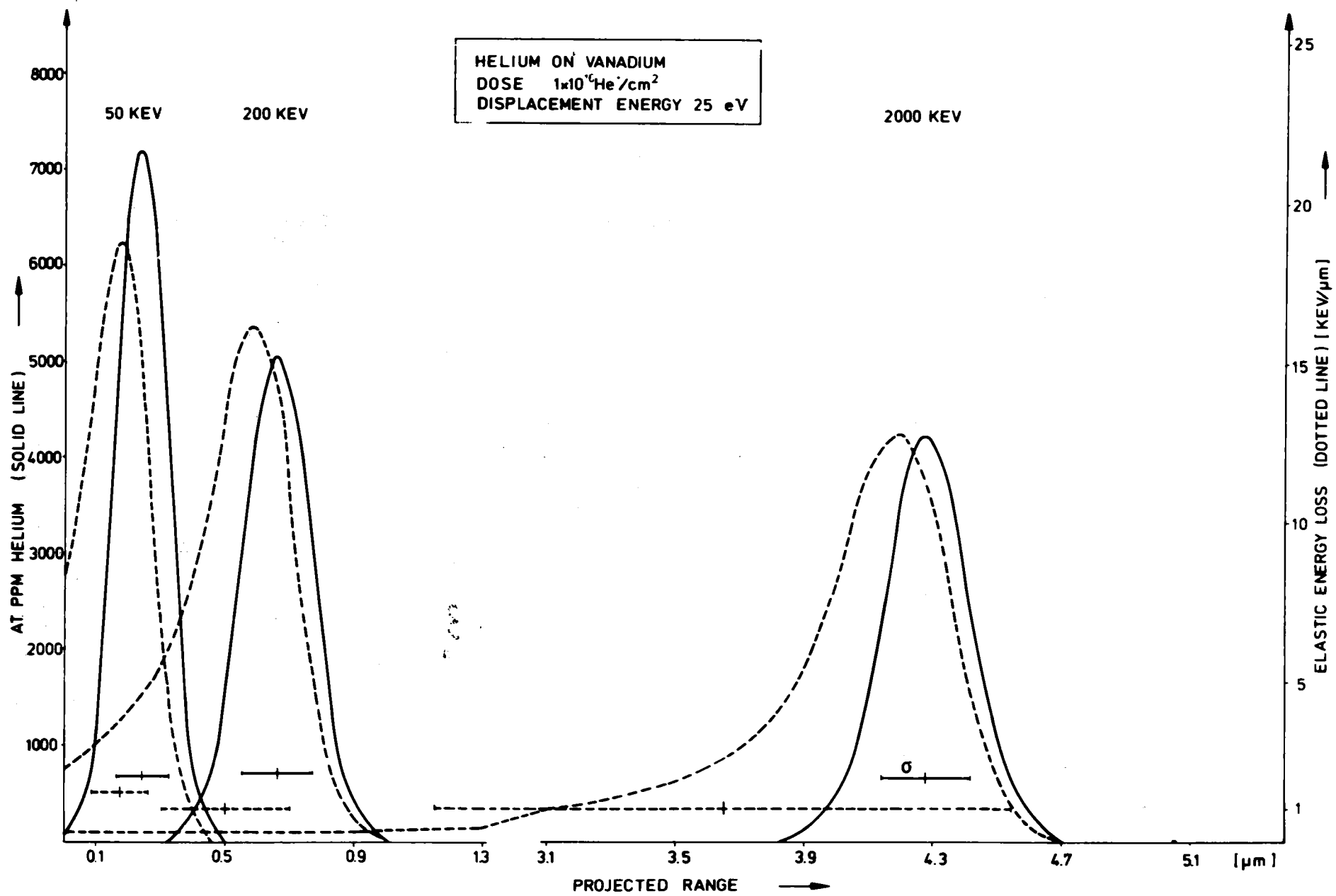


Fig. 4

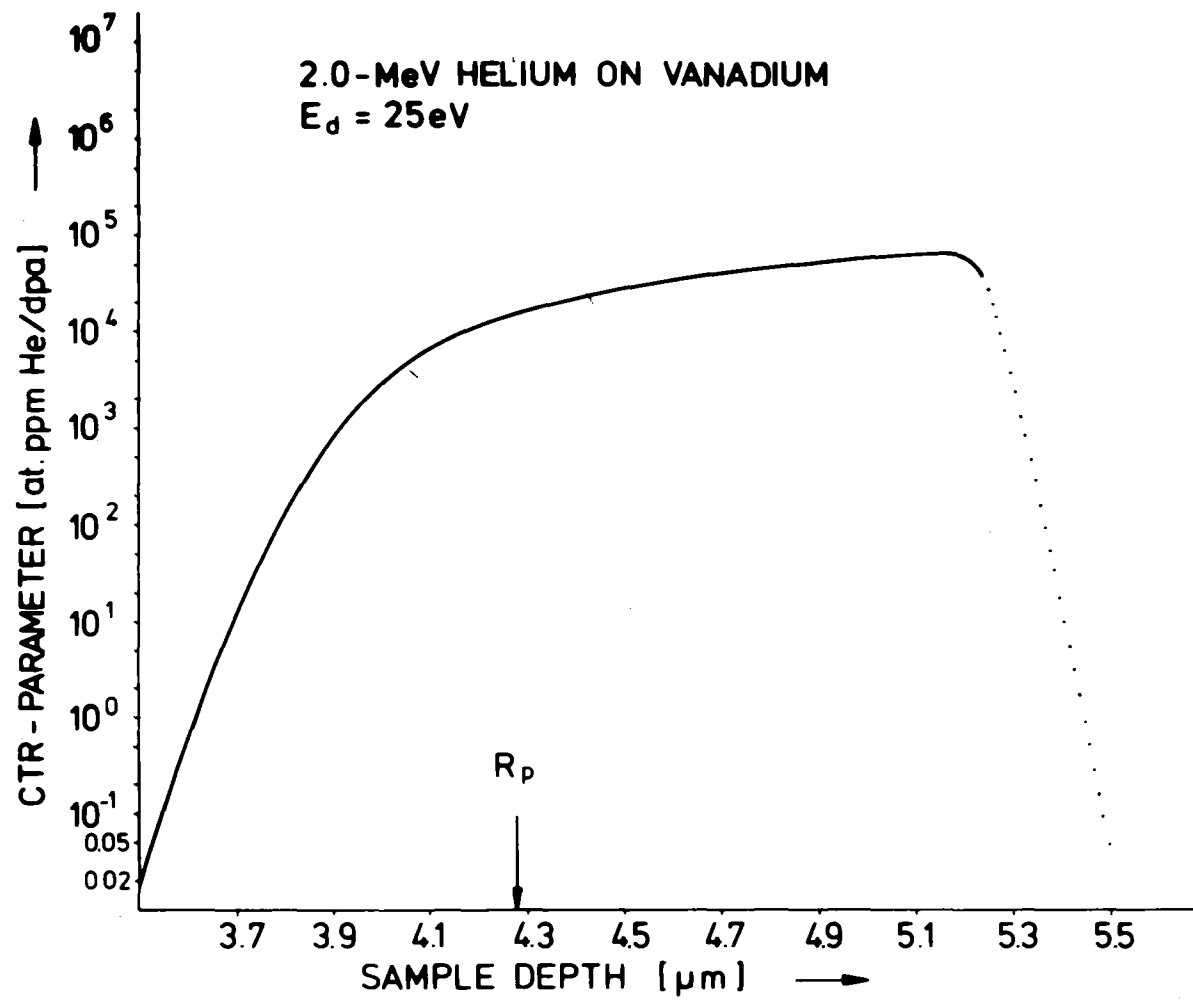


Fig. 5



CTR-PARAMETER VS SAMPLE DEPTH DOTTED LINE THERM. INDUCED DISPLACEMENTS ONLY.

D. KALETTA, IMF 2, 78-06-DK

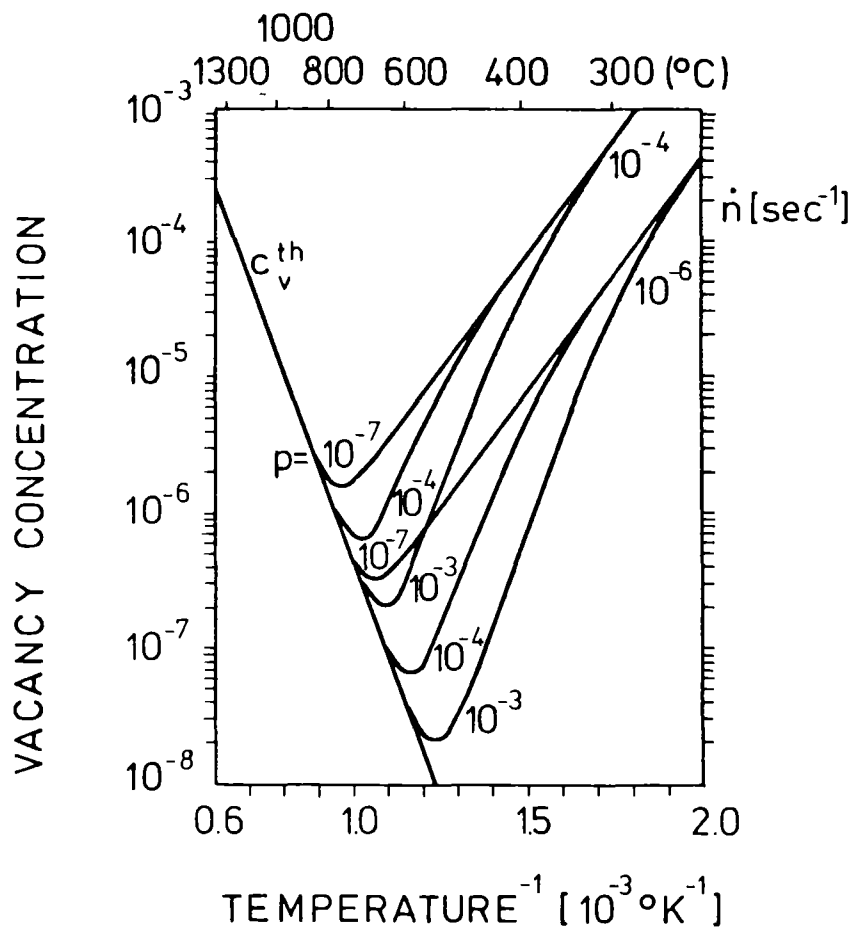


Fig. 6



STEADY STATE VACANCY CONCENTRATION AS FUNCTION OF INVERSE TEMPERATURE. THE DEFECT PRODUCTION RATES,  $\dot{n}$ , AND SINK ANNIHILATION PROBABILITIES,  $p$ , ARE GIVEN (AFTER WIEDERSICH 1972).

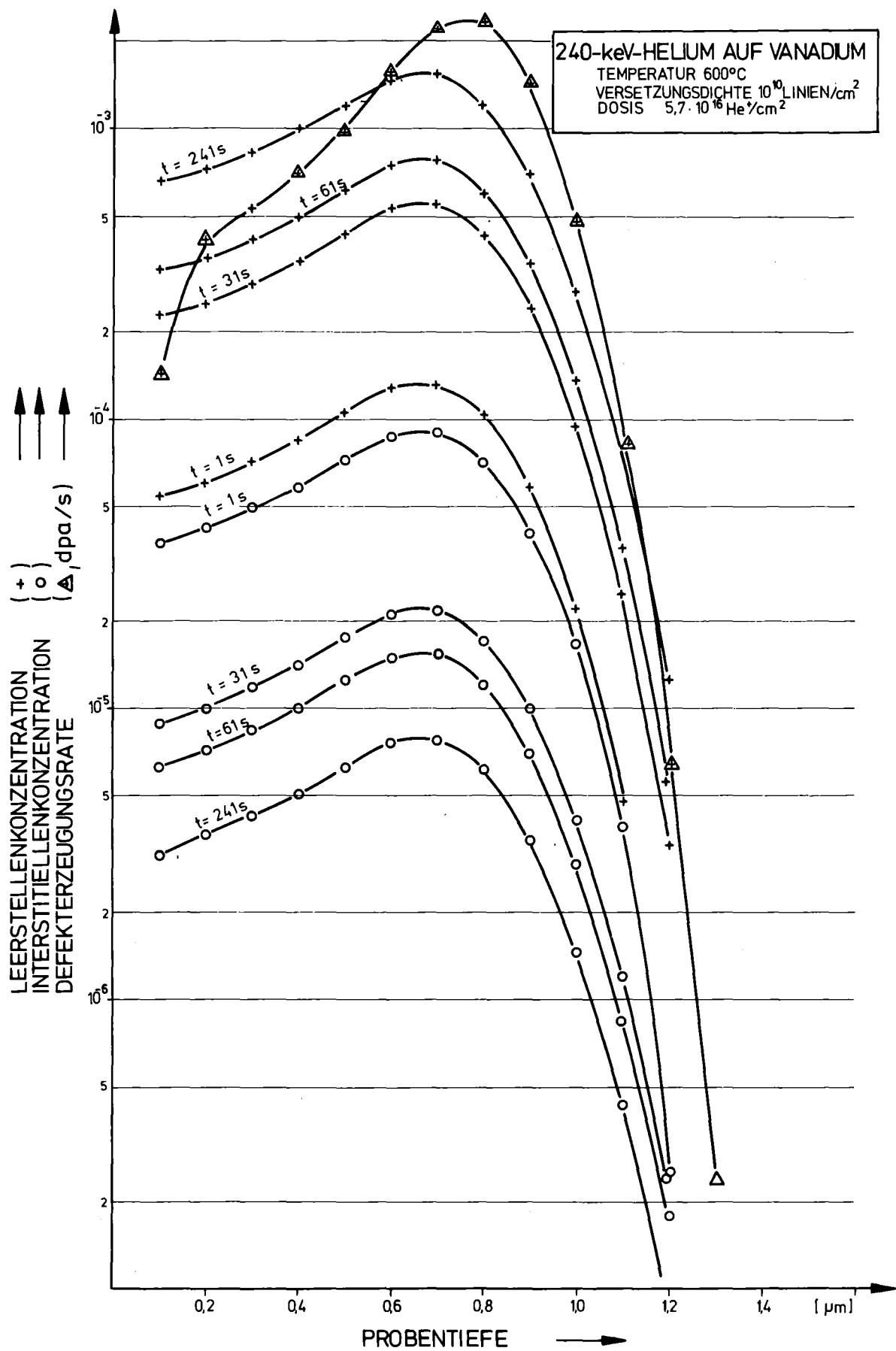
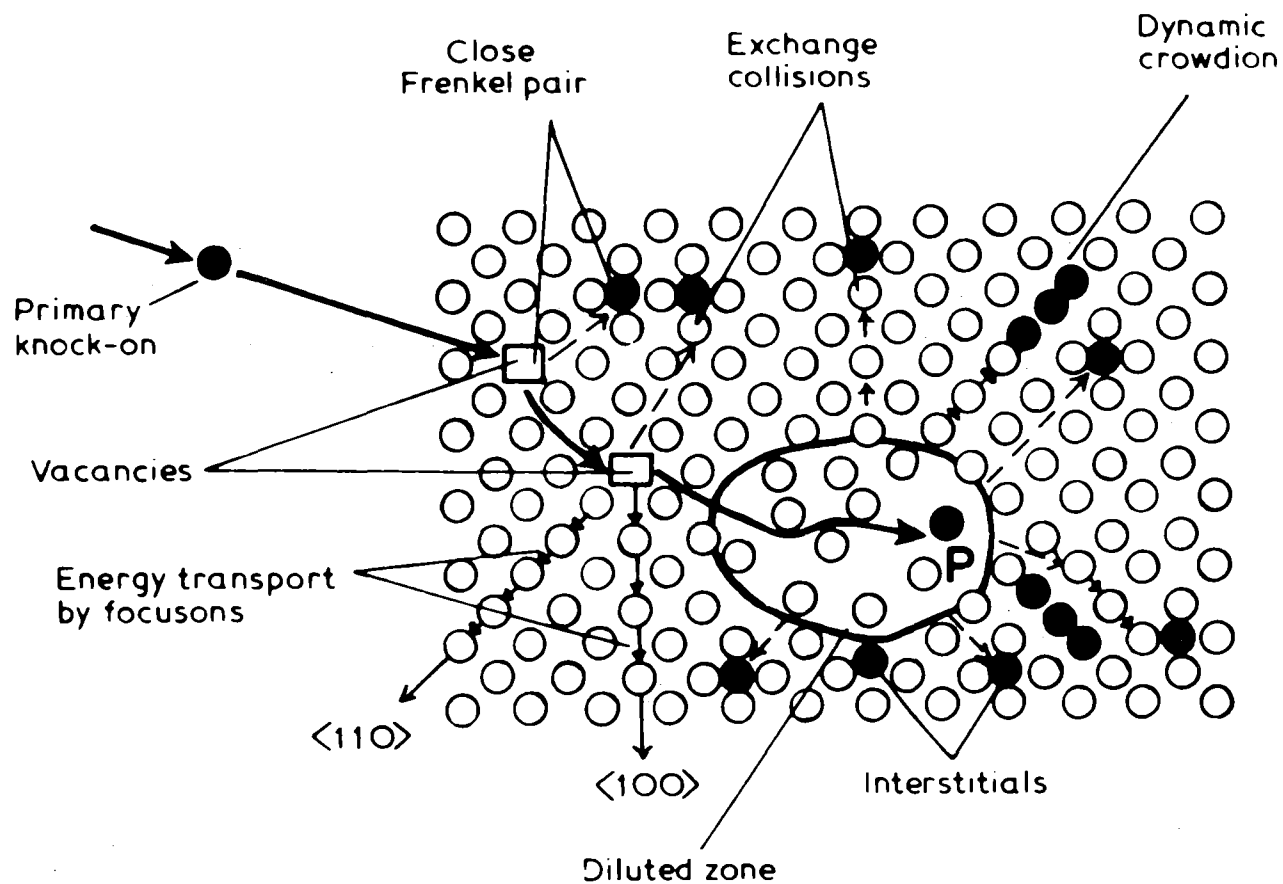


Fig. 7



*Figure 8.* Schematic two-dimensional representation of the Seeger depleted zone and its environment in a face-centred cubic crystal. A primary knock-on impinges from the left and comes to rest on the site P.

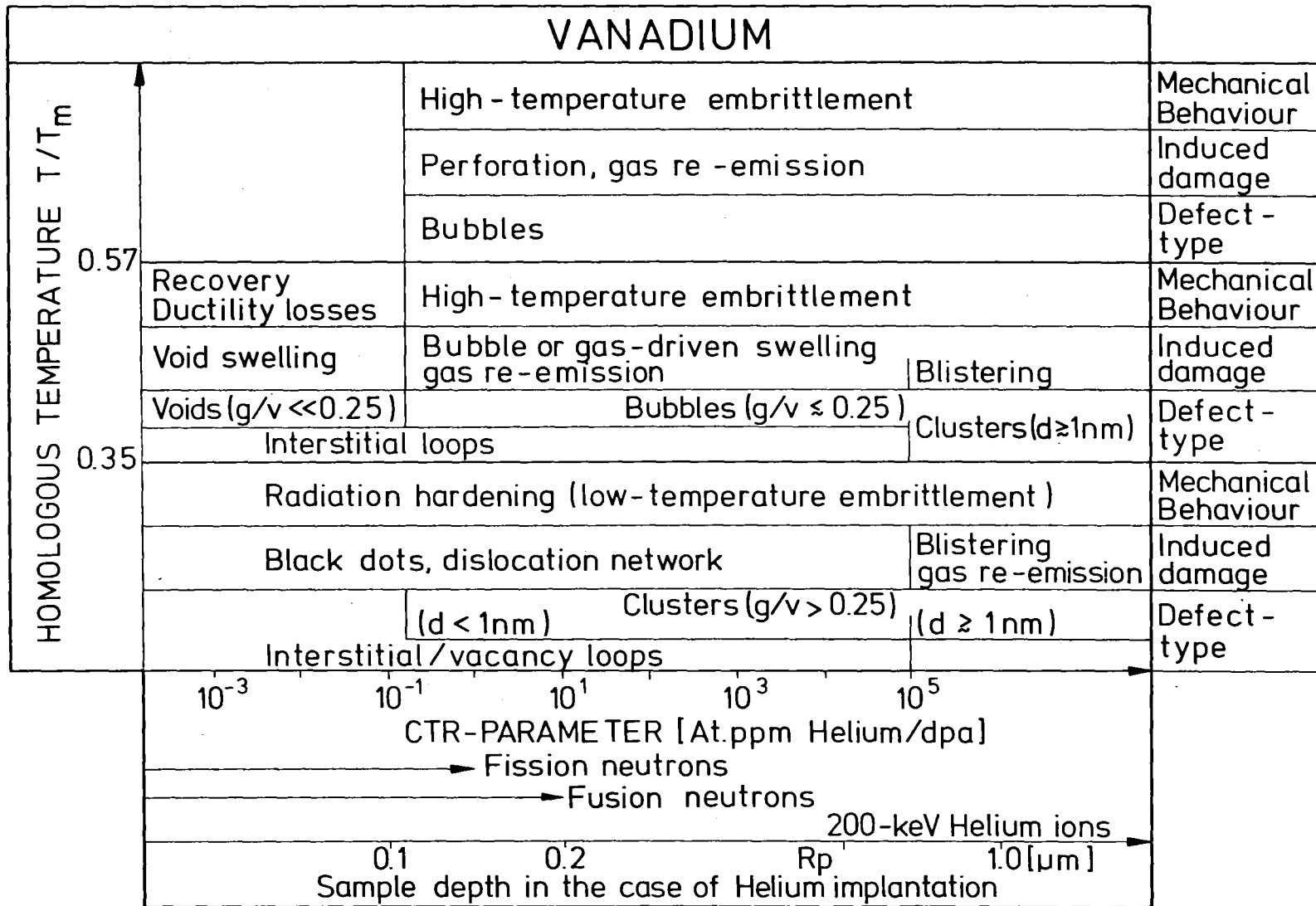


Fig. 9



THE DEFECT STRUCTURE IN VANADIUM AS A FUNCTION OF THE CTR-PARAMETER AND THE TEMPEPATURE (SCHEMATICALLY)  
 g = number of Helium atoms, v = number of vacancies, d = cluster diameter

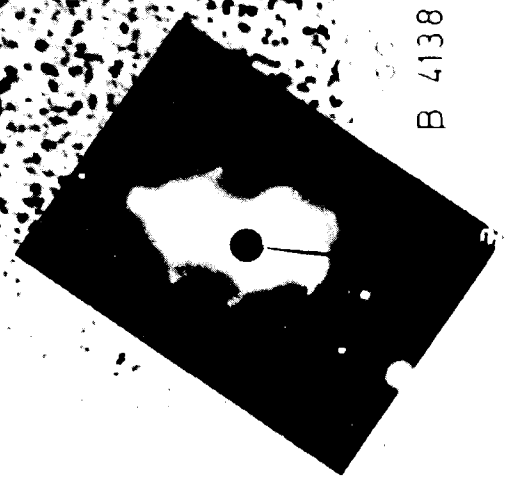
Ni  
DK 83-71  
He<sup>+</sup> Ni

Probe IX/K 5  
60 keV  
DOSIS 2.4 x 10<sup>16</sup> / cm<sup>2</sup>  
T<sub>irr</sub> 300 K

0.2 μm



50 000



B 4138

Fig. 10

6 - keV - HELIUM AUF VANADIUM

TEMPERATUR  $\approx 20^{\circ}\text{C}$

DOSIS  $6 \cdot 10^{17} \text{He}/\text{cm}^2$



— 2  $\mu\text{m}$

Fig. 11

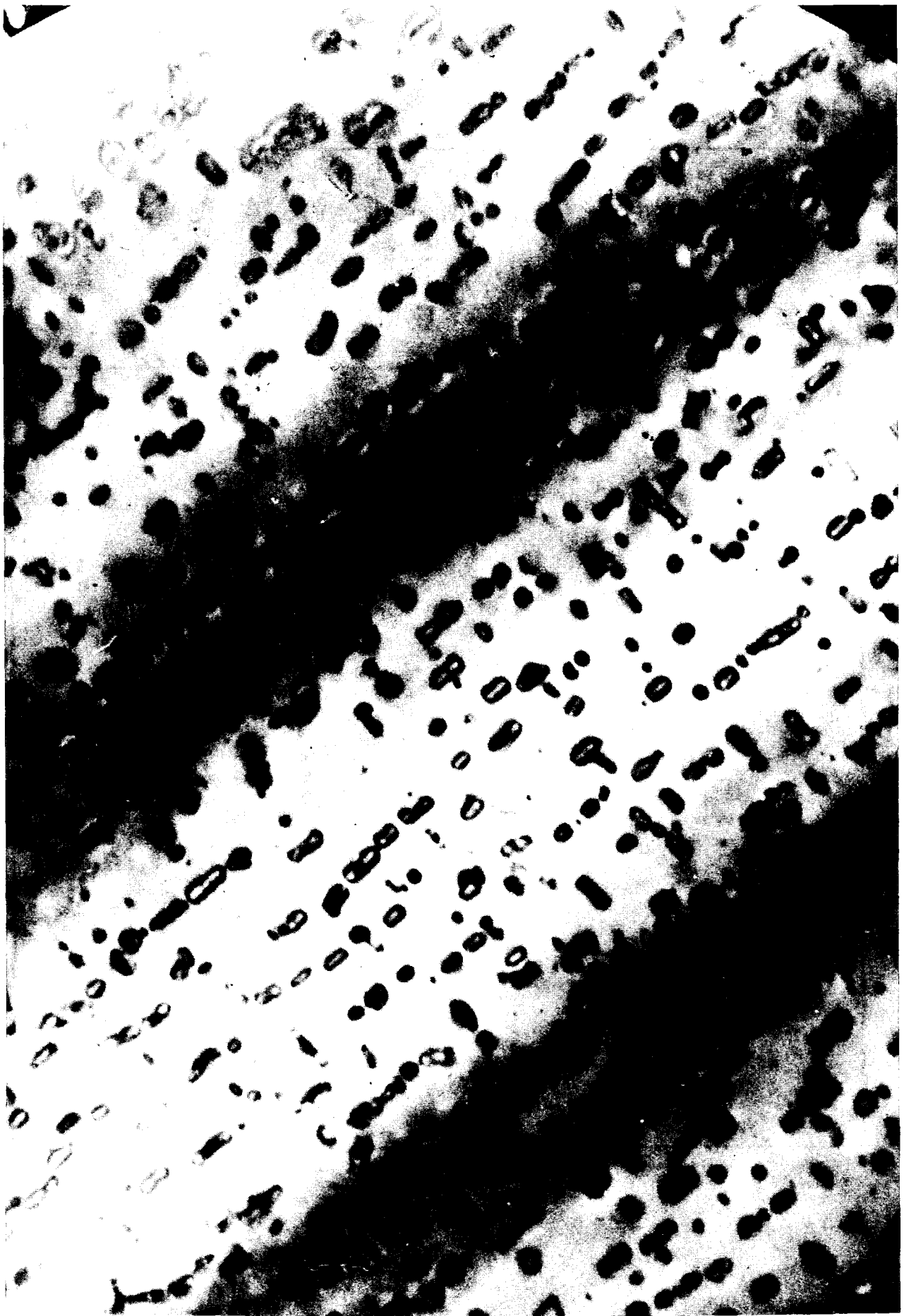
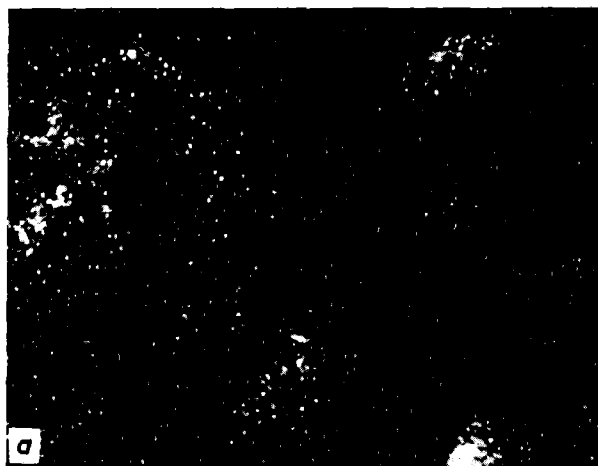
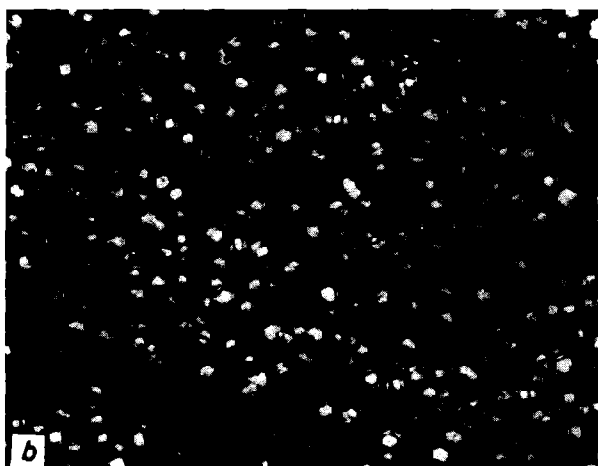


Fig. 12



T = 773 K



0.1  $\mu$

T = 848 K



T = 923 K

Fig. 13

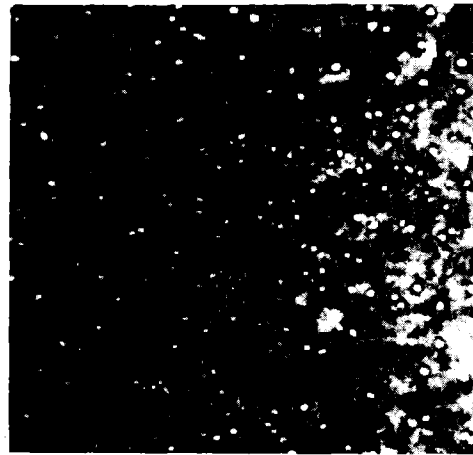
240-keV HELIUM ON ANNEALED VANADIUM  
IRRADIATION TEMPERATURE 575°C

DOSE  $5.7 \times 10^{16} / \text{cm}^2$

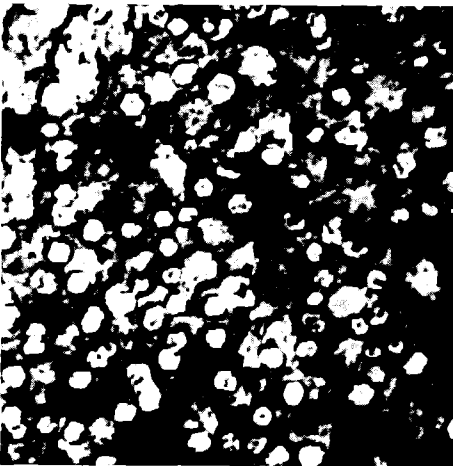
SAMPLE DEPTH a)  $0.6 \mu\text{m}$  b)  $0.8 \mu\text{m}$   
c)  $1.05 \mu\text{m}$  d)  $1.25 \mu\text{m}$



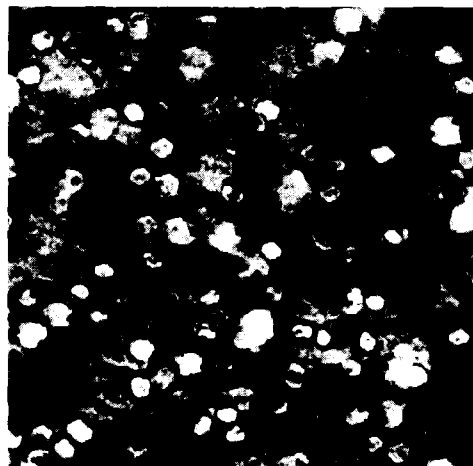
a)   $0.1 \mu\text{m}$



b)



c)



d)

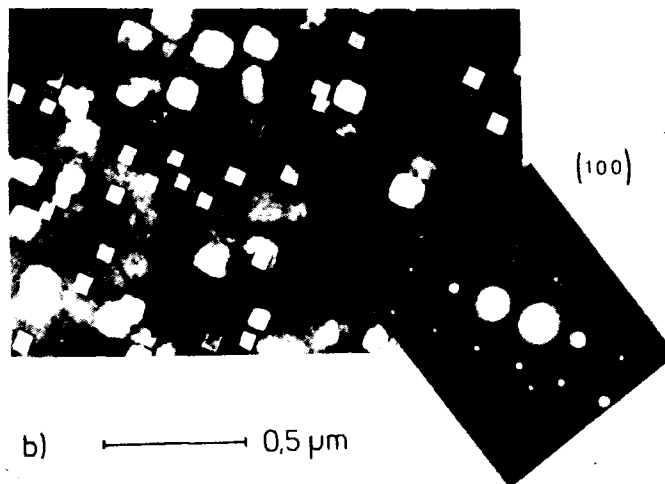
Fig. 14

2000 - keV HELIUM ON VANADIUM  
DOSE  $2 \times 10^{17} / \text{cm}^2$   
TEMPERATURE  $700^\circ \text{C}$

- a) SEM MICROGRAPH
- b) TEM MICROGRAPH OF THE SAME  
SAMPLE AT A DEPTH OF  $4.3 \mu\text{m}$



a)  $\longrightarrow$   $90 \mu\text{m}$



b)  $\longrightarrow$   $0,5 \mu\text{m}$

Fig. 15

104-MeV  $\alpha$ -PARTICLES ON VANADIUM ALLOYS

IRRADIATION TEMPERATURE 280°C

DOSE    •    10 At.PPM HE } HOMOGENEOUSLY  
          ▲    15At.PPM HE } DISTRIBUTED  
          ■    20At.PPM HE }

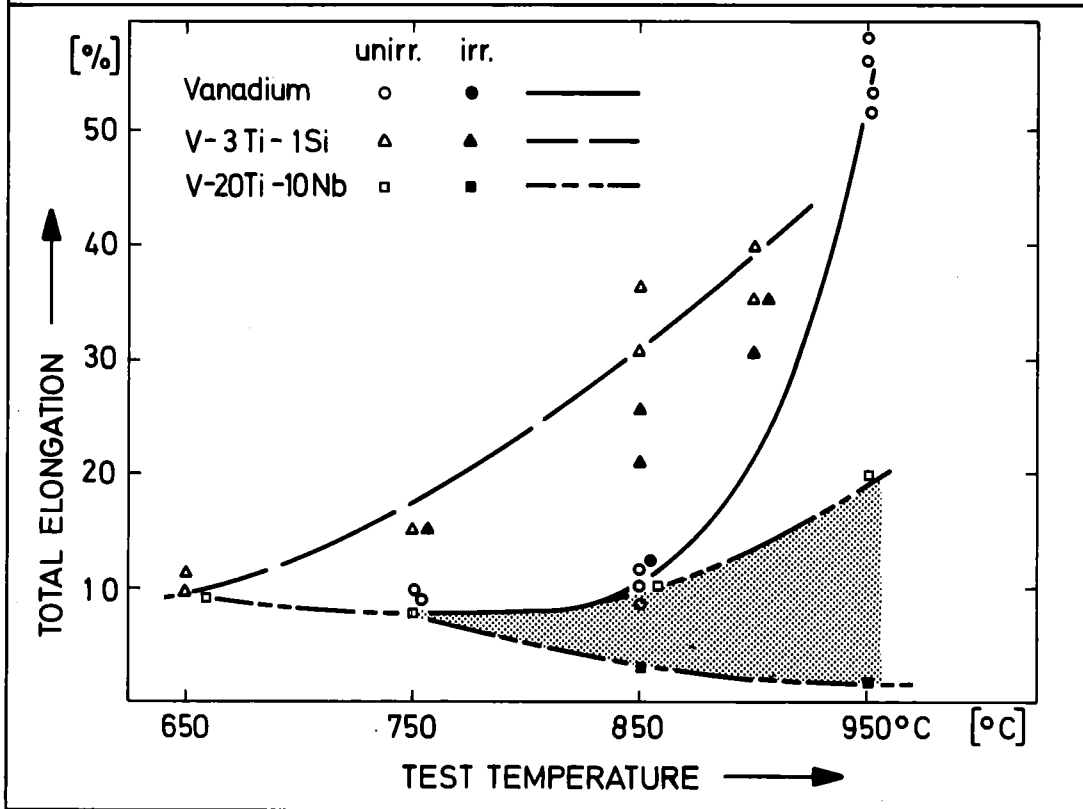


Fig. 16

210-keV-HELIUM AUF VANADIUM

DOSIS  $4 \cdot 10^{17} \text{He}^+/\text{cm}^2$

TEMPERATUR  $280^\circ\text{C} + \approx 1000^\circ\text{C}$

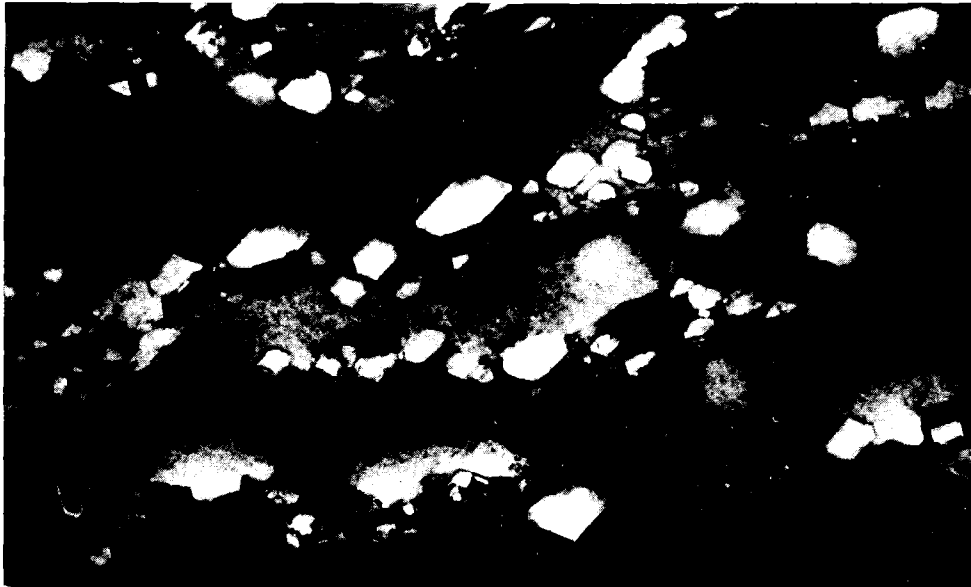


— 10  $\mu\text{m}$

Fig. 17

240-keV-HELIUM AUF V-20% Ti

TEMPERATUR 575° C  
DOSIS  $38,5 \times 10^{16}/\text{cm}^2$   
PROBENTIEFE a) 1,2  $\mu\text{m}$   
b) 0,8  $\mu\text{m}$



a)  $\longleftrightarrow$  0,2  $\mu\text{m}$



b)  $\longleftrightarrow$  0,2  $\mu\text{m}$

Fig. 18

# HELIUM - VACANCY CLUSTER (g,1) IN COPPER

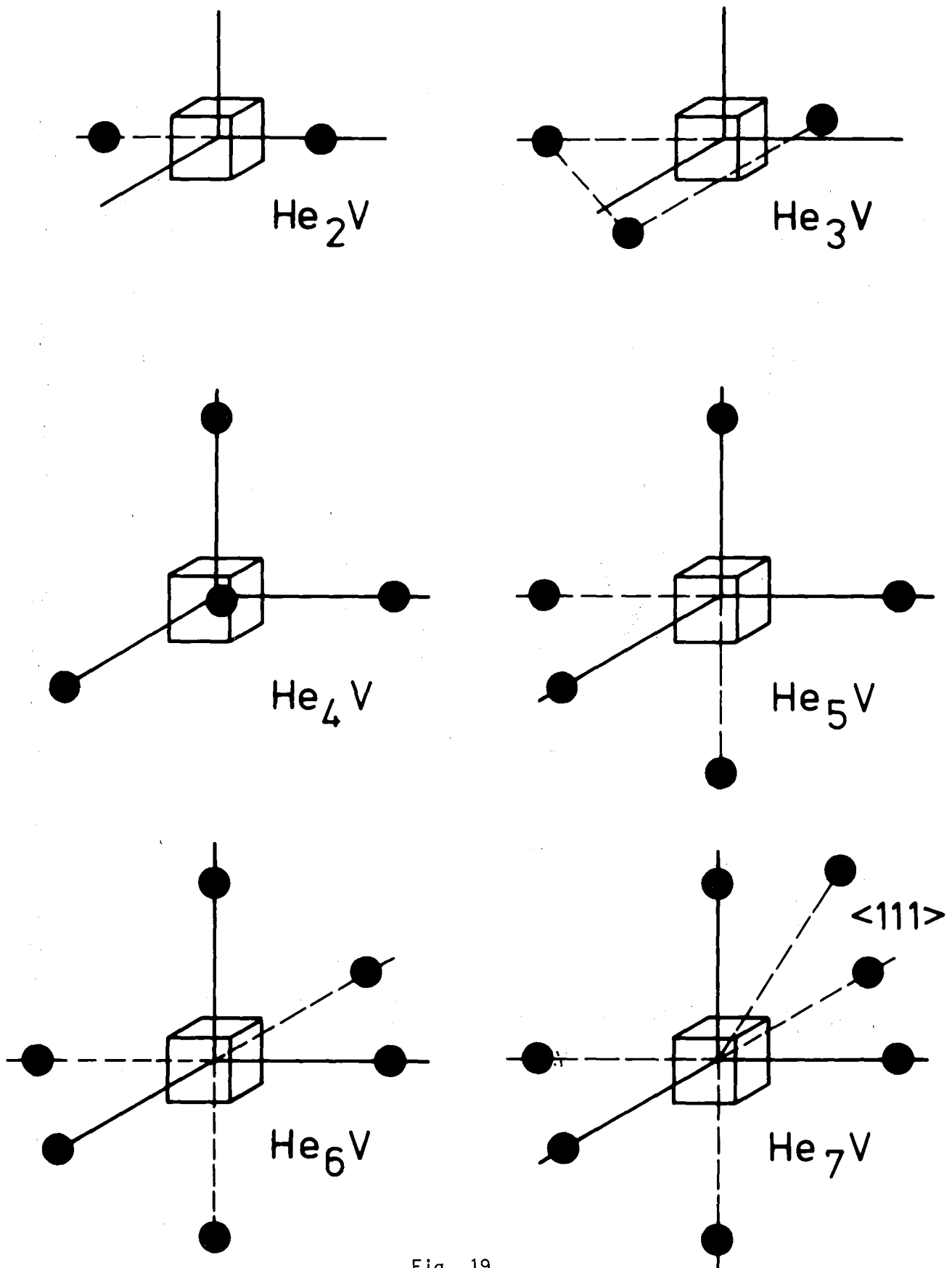


Fig. 19

RE-EMISSION RATE (PERCENT OF FLUX)

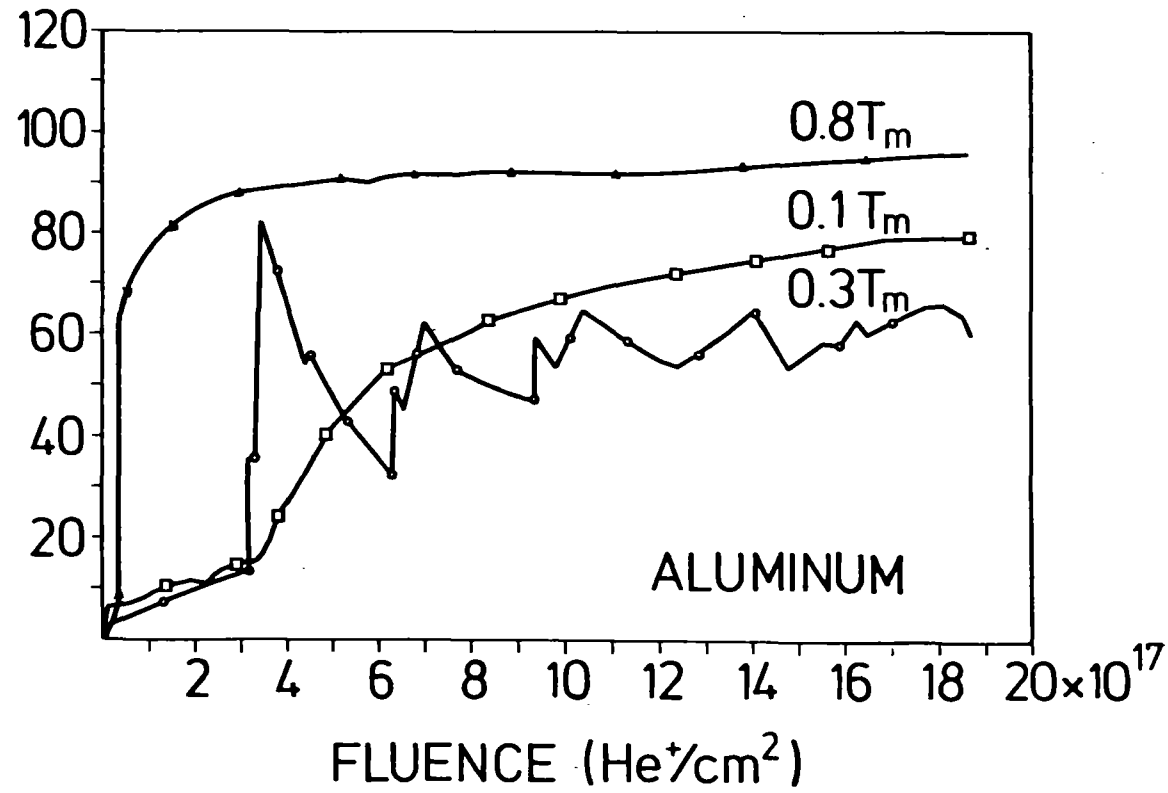


Fig. 20



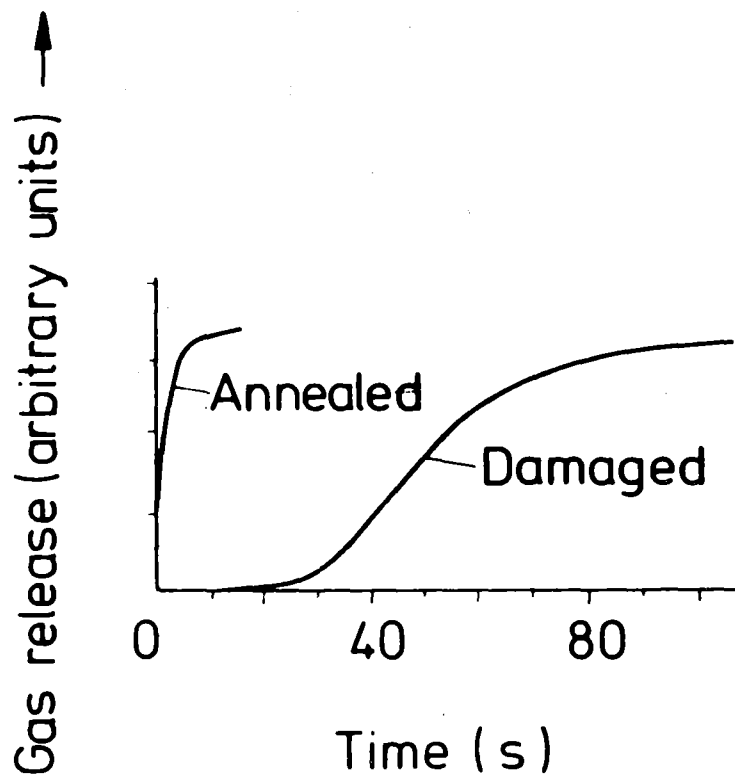


Fig. 21



GAS RELEASE DURING 20keV D<sup>+</sup> IMPLANTATION  
OF DAMAGED AND ANNEALED MO. (AFTER  
MC CRACKEN AND ERENTS 1973.)

DK 78 - 14

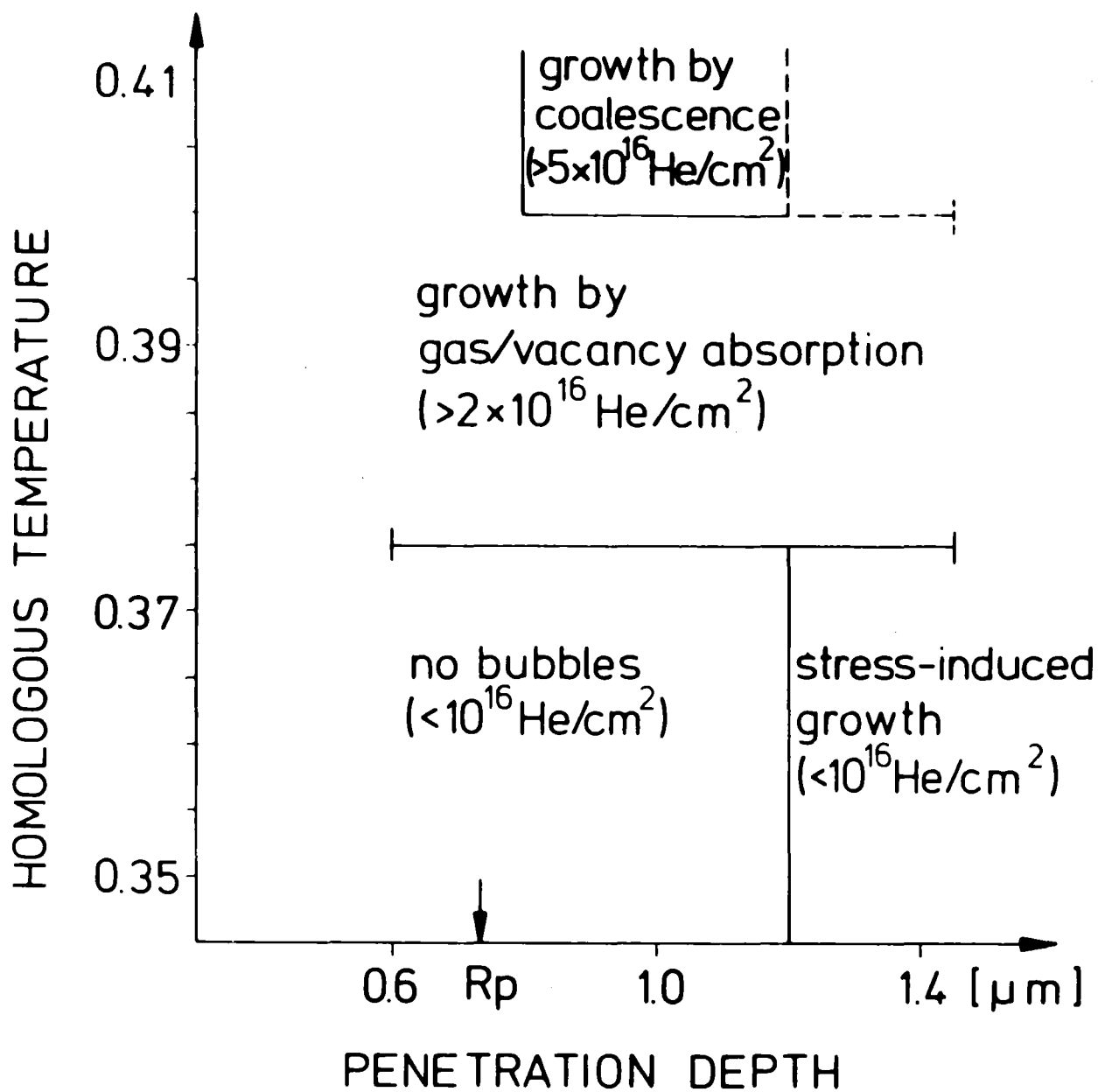
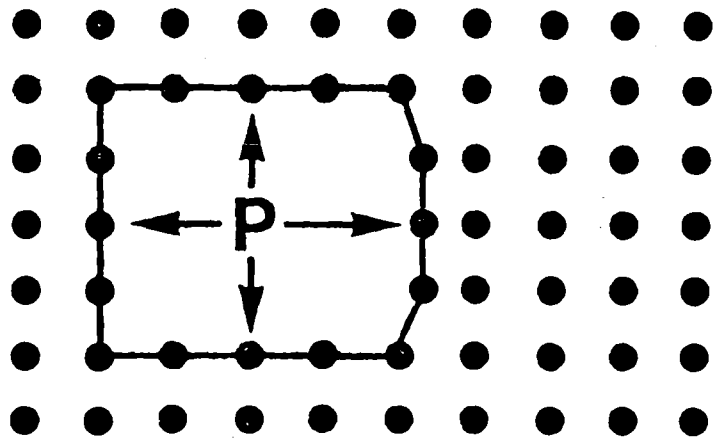


Fig. 22

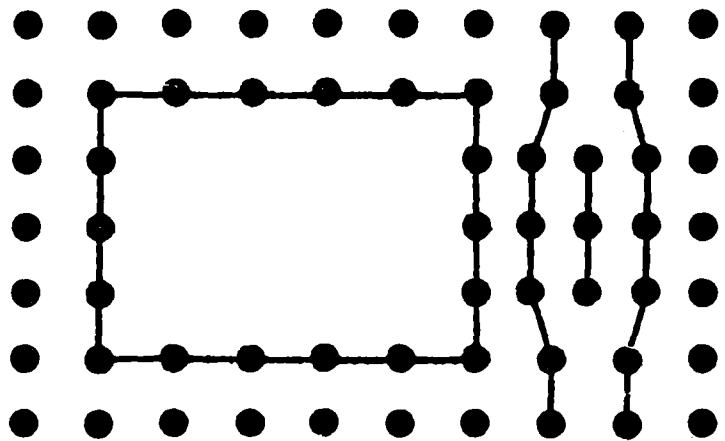


THE THREE MODES OF BUBBLE GROWTH IN VANADIUM  
 IM PLANTED WITH 240-keV HELIUM (SCHEMATICALLY)

D. KALETTA  
 DK 78-18



(a) EXCESS BUBBLE PRESSURE  
DEFORMS SURROUNDING ATOM  
PLANES.



(b) SHUNTING PROCESS ALLOWS  
EXPANSION OF BUBBLE AND  
CREATION OF INTERSTITIAL  
LOOP.

Figure 23. Mechanism of bubble growth by loop punching

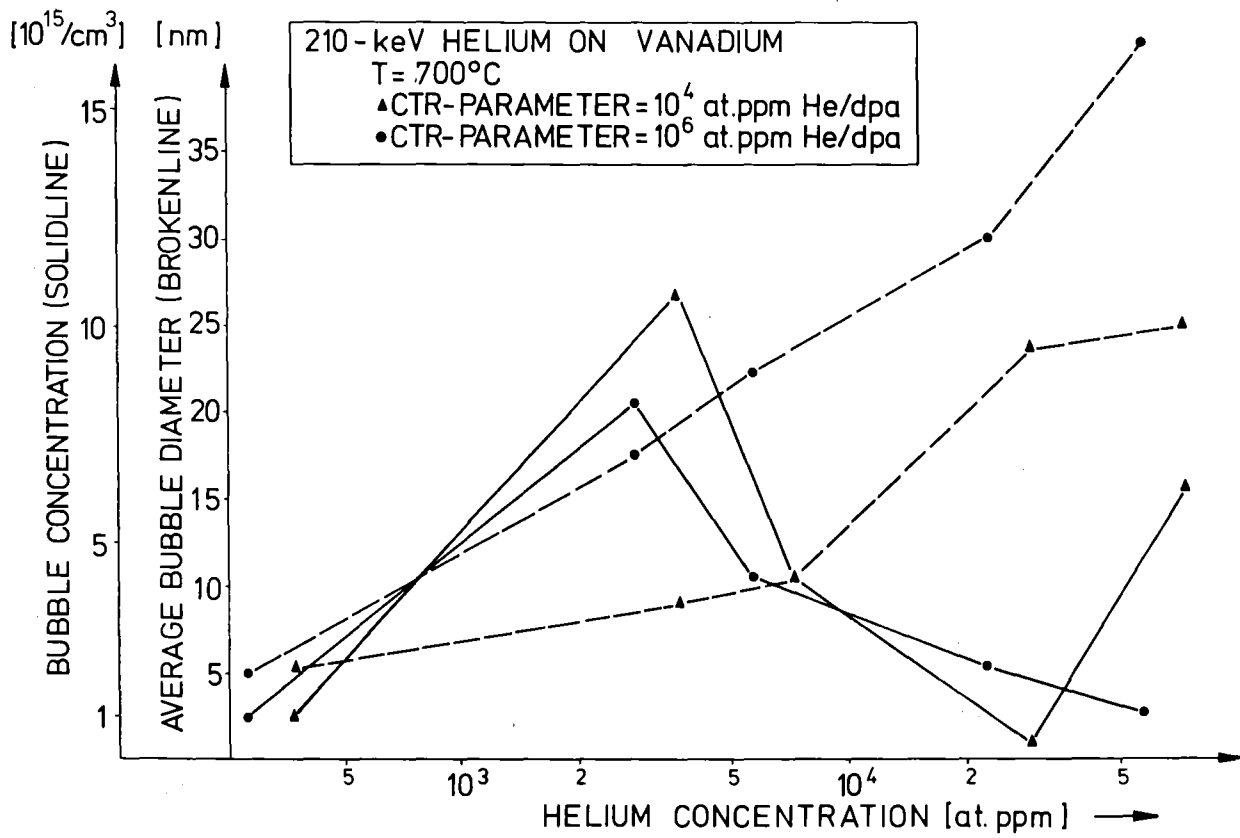


Fig. 24

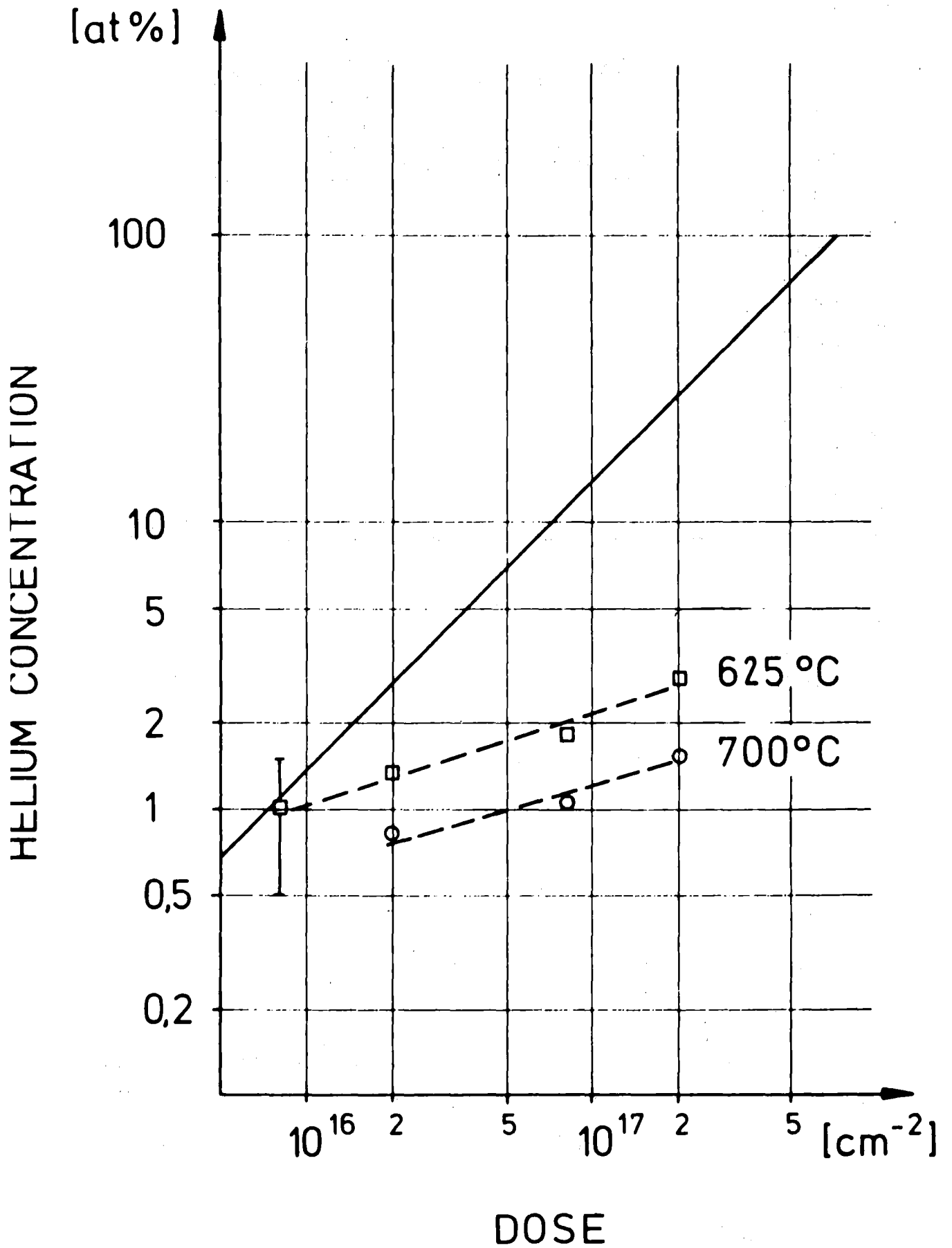


Fig. 25

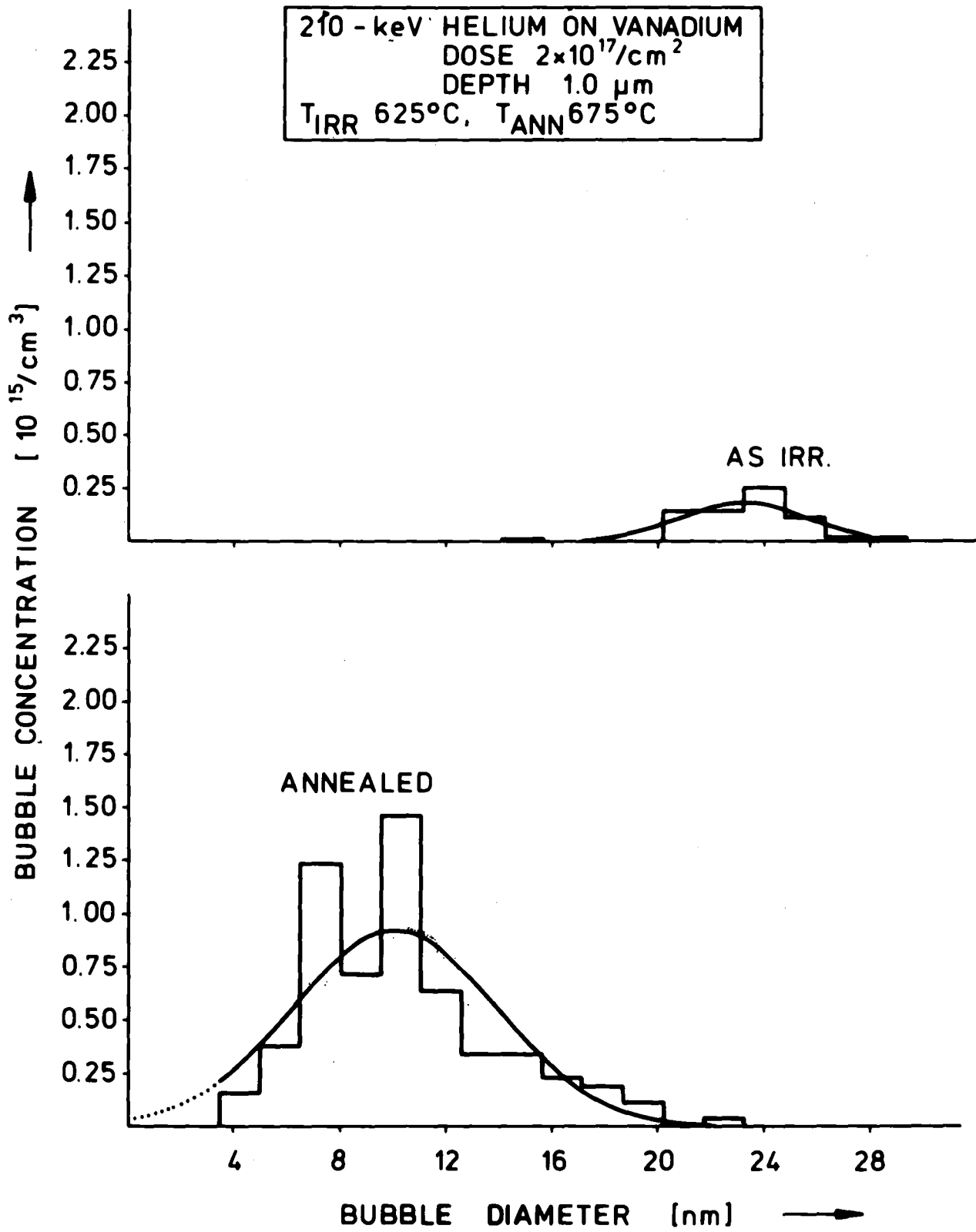


Fig. 26



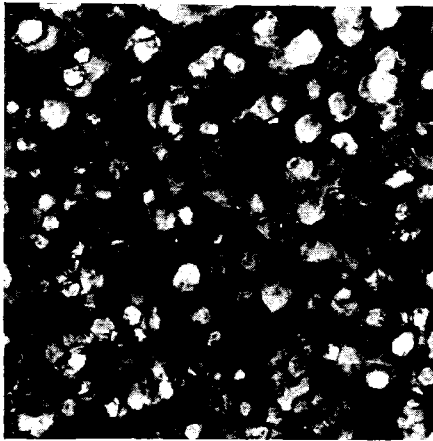
Fig.27. Electron micrograph illustrating the alignment of helium bubbles in molybdenum irradiated at  $300^{\circ}\text{C}$  with  $2.3 \times 10^{17}$  40 keV helium ions  $\text{cm}^{-2}$ . The orientation is close to (001).

240-keV-HELIUM AUF VANADIUM

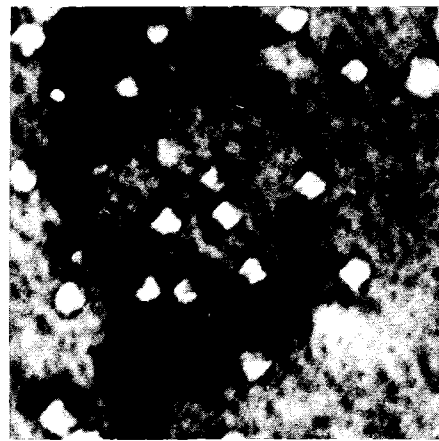
a,b) TEMPERATUR 625°C  
DOSIS  $2 \cdot 10^{17} \text{ He}^+/\text{cm}^2$

c,d) TEMPERATUR 700°C  
DOSIS  $8 \cdot 10^{16} \text{ He}^+/\text{cm}^2$

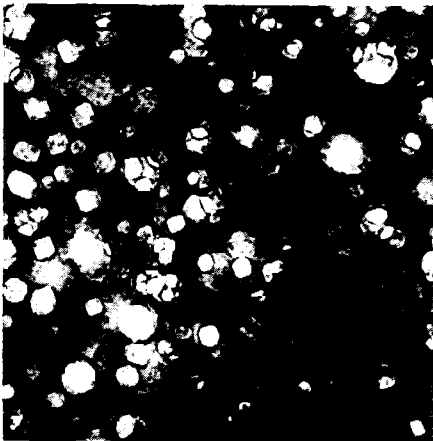
0,2  $\mu\text{m}$



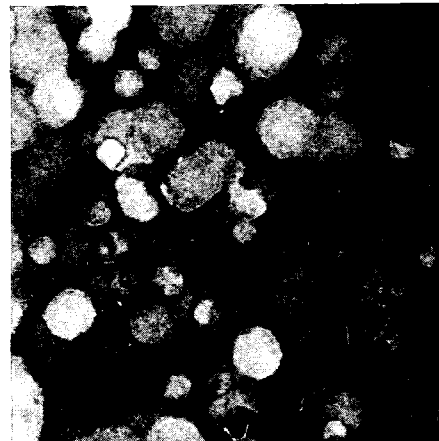
a)  $t = 318 \text{ s}$



b)  $t = 1830 \text{ s}$



c)  $t = 128 \text{ s}$



d)  $t = 580 \text{ s}$

Fig. 28

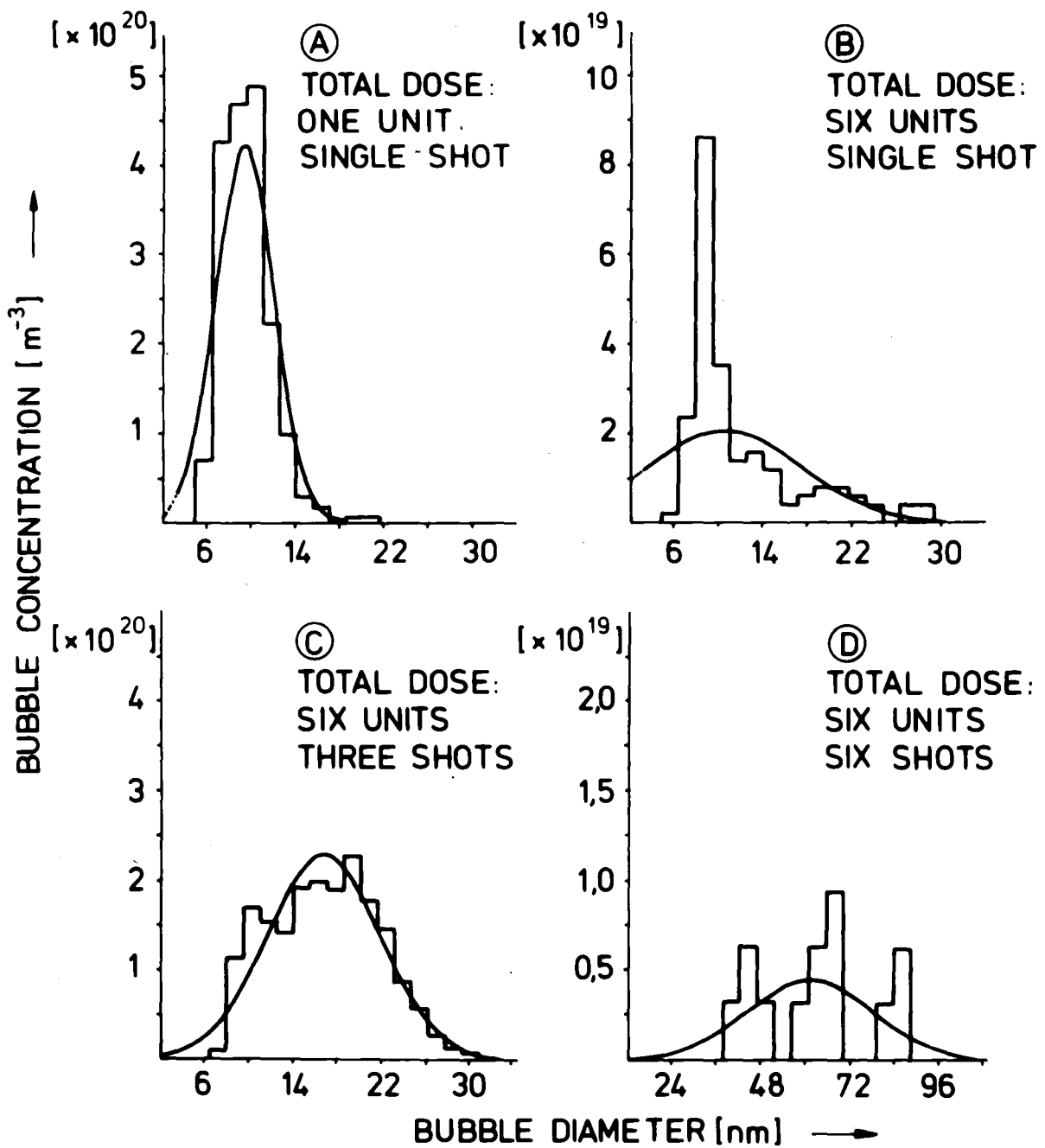


Fig. 29



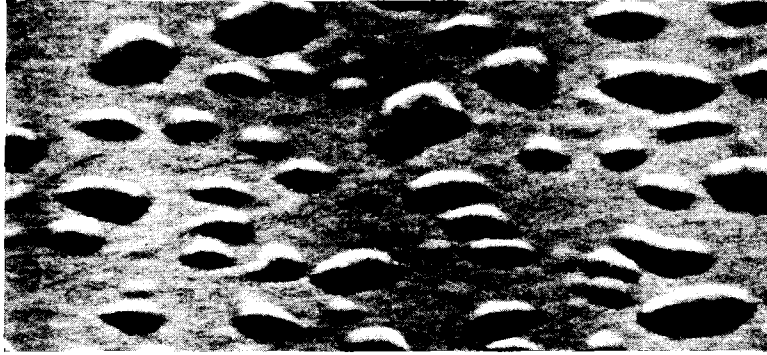
BUBBLE POPULATIONS OBTAINED FROM TEM - MICRO =  
 GRAPHS 2-MeV HELIUM ON VANADIUM,  $T = 848 \text{ K}$ ,  
 UNIT DOSE =  $93 \text{ C m}^{-2}$ , SAMPLE DEPTH =  $5.0 \pm 0.1 \mu\text{m}$

D KALETTA  
 IMF 2  
 78-03-DK

210-keV-HELIUM AUF V UND V-Ti-LEGIERUNGEN

TEMPERATUR 700° C

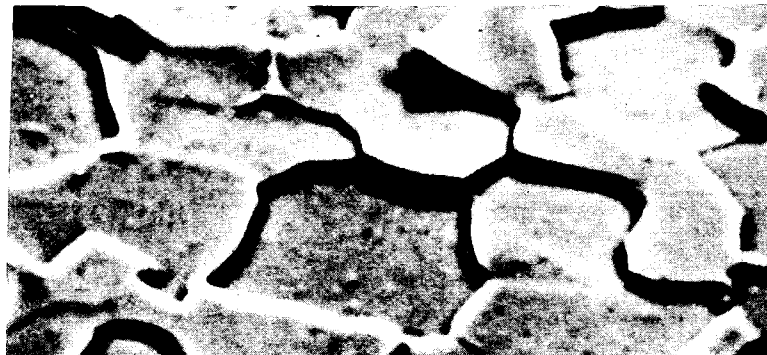
DOSIS  $8 \cdot 10^{17}$  He<sup>+</sup>/cm<sup>2</sup>



VANADIUM  20 μm



V-3GEW.% Ti  20 μm



V-20GEW.% Ti  10 μm

Fig. 30

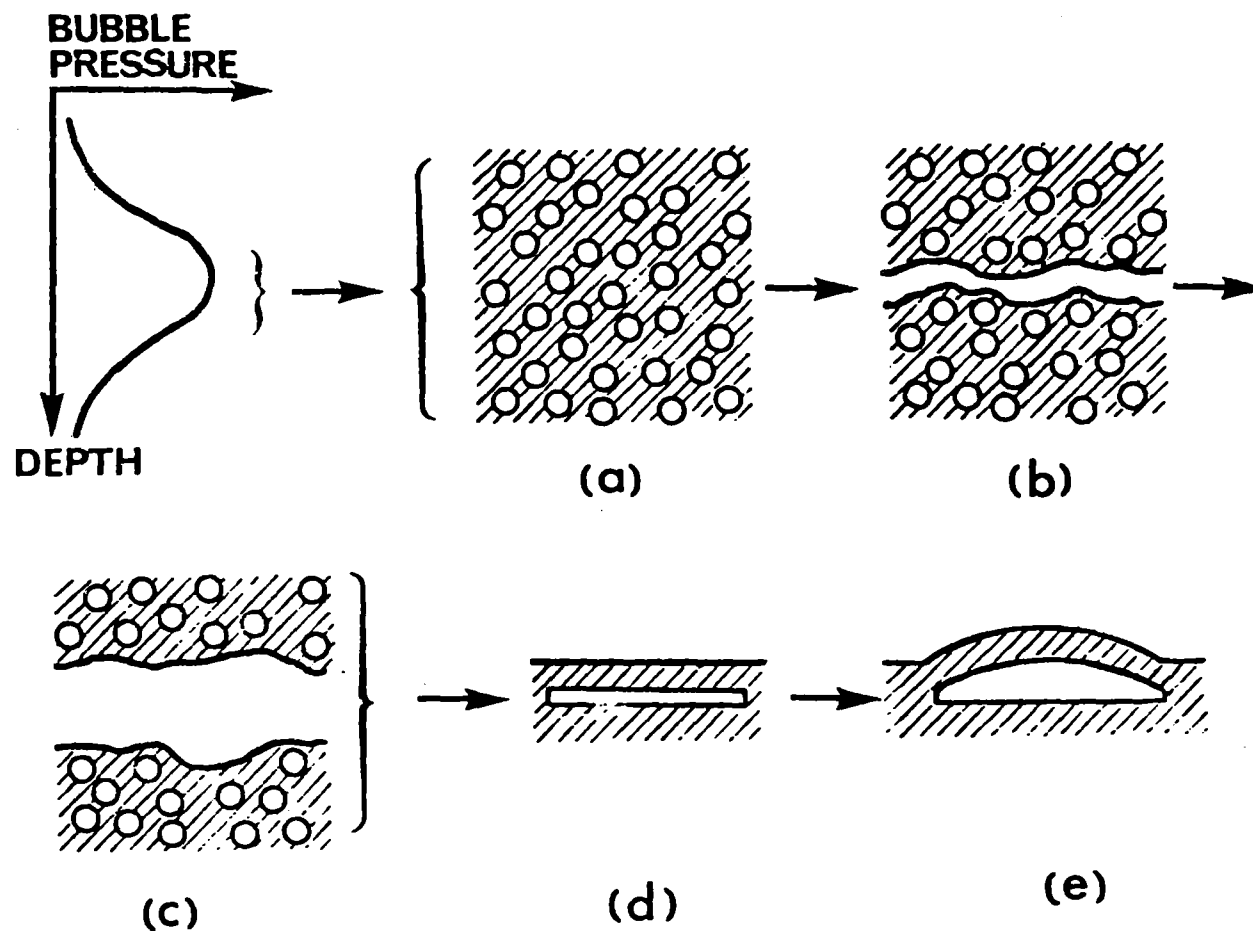


Figure 31. Interbubble fracture mechanism: (a) high density of overpressurised bubbles, (b) crack formation, (c) bubbles adjacent to original crack become involved to widen crack and increase pressure, (d) penny shaped crack which either extends to cause flaking or (e) forms blister by gas driven surface deformation.